Functionally Distinct pTfh1 Subsets with Roles in Malaria-Specific Immunity

Running title: Tfh cell diversity in human infection

Megan SF Soon [1], Damian A Oyong[1], Nicholas Dooley[1] , Reena Mukhiya[1,2,3], Zuleima Pava[1], Dean Andrew[2], Jessica R Loughland[1], James McCarthy[4], Jo-Anne Chan[1,4,5], James G Beeson[1,4,5], Christian Engwerda[2,3], Ashraful Haque[4], Michelle J Boyle[1,3,4,5 #]

1. Burnet Institute, 85 Commercial Road, Melbourne, VIC, Australia
2. QIMR-Berghofer, 300 Herston Road, Herston, QLD, Australia
3. Environment and Sciences, Griffith University, QLD, Australia
4. University of Melbourne, VIC, Australia
5. Monash University

corresponding author: michelle.boyle@burnet.edu.au

Conflict of interest statement: All authors declare no conflicts of interest

Abstract

Antibodies induced by infection or vaccination are essential mediators of protection. Induction of these protective responses is mediated by T-follicular CD4 T (Tfh) cells, and targeting these cells may be a strategy to boost antibody mediate protection. In humans, Tfh cells are analysed based on expression of CXCR3 and CCR6, with different subsets of Tfh (Tfh1, Tfh2, Tfh17) associated with antibody induction in a context-dependent manner. Here we dissected Tfh cells heterogeneity in healthy donors and individuals during controlled human malaria infection using scRNAseq. We identified two distinct Tfh1-like subsets with functional relevance, defined based on CCR7 expression. CCR7^{neg} Tfh1 cells express markers of cytotoxicity, while CCR7^{pos} Tfh1 cells produce reduced inflammatory cytokines and similar IL-21 resulting in unique cytokine milieu. In controlled human malaria infection, both CCR7^{pos} and CCR7^{neg} Tfh1, along with Tfh2 cells, clonally expanded and were transcriptionally and phenotypically activated. However, only CCR7^{pos} Tfh1 and Tfh2 cells associated with antibody development, suggesting a role for both these Tfh subsets in promoting humoral immunity to malaria. Data identify specific protective Tfh subsets that can be targeted to improve antibody mediated protection to malaria induced, and provide a frame work to dissect the role of Tfh subsets in other disease contexts.

44 **Introduction**

45 Antibodies and B cells induced by infection or vaccination are essential mediators of protection from
46 most pathogens. This includes malaria, caused by *Plasmodium falciparum* infection, which remains
47 one of the largest killers globally with >200 million cases and 600 000 deaths annually [1]. While the
48 introduction of two malaria vaccines, RTS,S/AS01 and R21/Matrix-M, bring new hope to malaria
49 control efforts, these vaccines only have modest and variable efficacy that is short-lived [2,3]. Antibody
50 development is driven by T-follicular helper (Tfh) cells, the key CD4 T cell subset that function
51 within the germinal centre to support B cell activation. Cytokine and receptor mediated signals from
52 Tfh cells, drive B cell selection, support antibody class switching, and differentiation into antibody-
53 producing long-lived plasma cells and memory B cells. As such, Tfh cells are attractive targets to
54 boost naturally acquired or vaccine-mediated protection and longevity [4]. To develop such therapies,
55 an improved understanding of how Tfh cells drive antibody development in malaria and specific
56 disease contexts is required.

57 Tfh cells, identified by expression of C-X-C chemokine receptor 5 (CXCR5) and programmed cell
58 death protein (PD1), are recognised to exist in distinct subsets, which have specific and context
59 dependent roles in antibody induction. These Tfh subsets take on characteristics of CD4+ T cell
60 helper cell lineages [5], and are commonly analysed by CXCR3 and CCR6 expression to identify Tfh1
61 (CXCR3+/CCR6-), Tfh2 (CXCR3-/CCR6-) and Tfh17 (CXCR3-/CCR6+) cells, both in the periphery
62 and also in (GC) Tfh cells in secondary lymphoid tissues [6]. The development and activation of Tfh
63 subsets may be underpinned by 'skewing' of Tfh cells by the cytokine milieu induced during infection
64 or vaccination, allowing Tfh cells to adopt specific roles to influence B cell development [5,7]. Indeed,
65 defined Tfh cell subsets have differing abilities to activate naïve or memory B cells and have been
66 associated with antibody development in a pathogen and vaccine-dependent manner. For example,
67 Tfh2 cells have the highest capacity to activate naïve B cells, and peripheral (p)Tfh2 cells have been
68 associated with the development of broadly neutralizing antibodies in HIV infection [8]. On the other
69 hand, Tfh1 cells robustly activate memory B cells, and the activation of pTfh1 cells are consistently
70 associated with antibodies induced by influenza vaccination [9,10]. Thus, development of strategies to

target Tfh cells to boost antibody development require a context specific and in-depth understanding of specialised Tfh subsets that drive protective antibodies.

In malaria, progress has been made to define roles of Tfh cells in antibody development in infection and vaccination [11]. Studies by our team have shown that the activation of pTfh2 cells was associated with antibody development during controlled human malaria infection (CHMI) with *P. falciparum* [12]. Similarly, others have shown that pTfh2 cells are associated with induction of antibodies by approved and experimental malaria vaccines [13–15]. These association are observed despite the overall response during malaria being dominated by pTfh1 cells [12,16,17]. Further, in Malian children, pTfh1 cell activation was not associated with antibody development following malaria treatment [17], and pTfh1 cells have been associated with induction of short-lived plasma cells which may hamper the germinal centre [12,18]. As such, data suggests that strategies that can boost Tfh2 and reduce Tfh1 activation may improve malaria antibody development. However, recent studies by our team have shown that these relationships are more nuanced, with Ugandan children who had the highest levels of protective antibodies having increased frequencies of activated pTfh2 and pTfh1 cells [19]. Additionally, parasite activated pTfh1 cells induced T-bet+ B cells with high IgG3 expression [20], and IgG3 antibodies are consistently associated with protection from malaria [21]. To develop Tfh cell targeted approaches to improve malaria antibody development and longevity in infection and vaccination, an increased understanding of the specific Tfh cells that drive protective antibodies is required.

We hypothesised that contradictory results may be in part due to the limited approaches to identify subsets of Tfh cells, and an improved understanding of Tfh heterogeneity would reveal protective subsets associated with antibody development in malaria. In this study, we applied scRNAseq and spectral flow cytometry to unique clinical cohorts to discover functionally relevant Tfh cell subsets that have differing roles in malaria antibody development. We identify two transcriptionally and phenotypically distinct pTfh1 subsets in healthy individuals which can be identified based on CCR7 expression, with differences in expression of cytotoxic markers and cytokine production. Tracking pTfh cell activation with sc-RNA/VDJ-seq during CHMI, we show Tfh subset specific activation and clonal expansion, with increased activation and clonal expansion of pTfh1 CCR7^{pos} compared to other

98 subsets. Finally, we show that antigen specific pTfh1 CCR7^{pos} cells, along with pTfh2 cells, but not
99 pTfh1 CCR7^{neg} cells associated with development of functional and protective antibodies following
100 malaria. Our data explain previous contradictions in the field and highlight the phenotypic and
101 functional diversity of Tfh cells during human infection. Data open new avenues to develop
102 approaches which harness Tfh cells to enhances vaccine efficacy and improve antibody development
103 and protection.

104

105 **Results**

106 **Analysis of Tfh cells with scRNAseq identifies two Tfh1-like subsets**

107 We hypothesised that hidden diversity of Tfh cells with distinct functional capacity, not captured in
108 traditional analysis methods, underpinned the unclear roles of Tfh subset in antibody development in
109 malaria. To dissect this diversity and identify protective Tfh subset that drive malaria antibody
110 development we first performed scRNAseq on pTfh cells sorted from healthy human donors (n=4, sex
111 50% males, aged 28.5 [25.5-35], median [IQR] years). To understand the link between commonly
112 identified Tfh cells and potential hidden diversity, we sorted three Tfh subsets (pTfh1, pTfh2 and
113 pTfh17 from CXCR5+ PD1+ cells), based on classical definitions of CXCR3/CCR6 expression,
114 alongside the less functional or less activated CXCR5+ PD1- compartment (**Fig. 1A, Supplementary**
115 **Fig. S1A**). After QC, a total of 7,302 cells were analysed with high quality cells captured from each
116 donor and subset (pTfh1 n= 2,089, pTfh2 n=717, pTfh17 n=744, PD1- n=2,839, **Supplementary Fig.**
117 **1B**). Following data integration by donor (**Supplementary Fig. 1C)**, we identified 11 Tfh cell clusters
118 using a combination of unsupervised and semi-supervised clustering methods (**Fig. 1B-D,**
119 **Supplementary Table 1**). Strikingly, two distinct Tfh1 clusters were identified, both with relatively
120 high expression of *CXCR3* and *CST7* (annotated Tfh1_cytotoxic and Tfh1_CCR7). A Tfh2 cluster
121 was identified with high expression of genes associated with GC Tfh cells, including *TOX2* [22,23], *MAF*
122 [24,25], and *TCF7*. The signature of this cluster mapped to the majority of tonsil GC Tfh cells in a
123 publicly available data set [26] (**Supplementary Fig. 1D**), confirming the transcriptional relationship

124 between Tfh2 cluster and GC Tfh cells identified here and reported previously [8]. Tfh17 cluster was
125 annotated based on high expression of genes associated with Th17 cells *CCR6, BHLHE40,* and
126 *TGFB1* [27–29]. Most cells within these Tfh1/Tfh2 and Tfh17 transcriptional clusters were sorted from
127 the PD1+ cells (**Fig. 1B/C**). Other transcriptional clusters included cells enriched in Type I IFN genes
128 (annotated as IFNI), a cluster enriched with heat shock proteins (annotated stress), another cluster
129 enriched with ribosomal genes (annotated ribosomal), and two clusters without clear marker genes
130 (cluster 2, possibly a quiescence cell subset, with upregulation of genes *BTG1* and *ZFP36L2,* and
131 cluster 3 which only had limited upregulated genes including annexin family members *ANXA1*,
132 *ANXA2*, *S100A10)* (**Fig. 1D**). Analysis of key T helper genes also identified a small cluster of cells
133 positioned close to the Tfh1 cluster that expressed a mixture of Tfh1/Tfh17 signature, which were
134 manually clustered and annotated as Tfh1.17 (**Fig. 1B/D**). Additionally, another subset of cells
135 expressing *FOXP3* and Treg signature genes including *CTLA4* was identified manually and annotated
136 as Tfr (**Fig. 1D**). The remaining Tfh cell subsets expressed diverse levels of markers associated with
137 various aspects of Tfh or CD4 T cell development, with no clear patterns of expression across subsets
138 (**Supplementary Fig. 1E**).

139 Comparing the two cell clusters identified as Tfh1 cells, the Tfh1_cytotoxic cluster had high
140 expression of *GZMK*, *GZMM*, *CCL5* and *NKG7* (**Fig. 1D/E, Supplementary Fig. 1E,**
141 **Supplementary Table 2)**. The signature of the Tfh1_cytotoxic annotated cells overlaps with
142 cytotoxic Tfh cells previously identified in mice models, including the increased expression of
143 *EOMES* [30], and in a recent small analysis of human Tfh cells from the periphery and tonsil
144 [31] (**Supplementary Fig. 1E)**. Potentially cytotoxic, granzyme-K expressing pTfh cells have also
145 recently been identified in type-1 skewed response in mice, and in human CMV specific pTfh cells [32].
146 In contrast, the Tfh1_CCR7 cluster had lower expression of cytotoxic markers, and instead had
147 increased expression of *CCR7* and *SELL.* Differential expression of CCR7 along with PD1 has
148 previously been used to differentiate Tfh subsets within CXCR5+ cells in both mice and humans, with
149 $CCR7^{lo}/PD1^{hi}$ described as effector cells and $CCR7^{hi}/PD1^{lo}$ described as resting cells [33]. However
150 here, both Tfh1_cytotoxic and Tfh1_CCR7 subsets largely existed in clusters that were from the

151 PD1+ sorted populations thus identifying an unappreciated gradient of CCR7 expression within PD1+
152 cells (**Fig. 1C/F, Supplementary Fig. 1F).** Pathway analysis of Tfh1_CCR7 and Tfh1_cytotoxic
153 cluster marker genes highlighted the shared and divergent transcriptional signatures of these cells
154 (**Supplementary Fig. 1G**). For example, both subsets were enriched for 'Th1 pathway', and
155 'Interferon gamma signalling', while only Tfh1_CCR7 cells were enriched in 'Th2 pathway' and
156 'ICOS-ICOSL Signalling in T Helper Cells' suggesting potential functional differences between the
157 two transcriptional clusters (**Supplementary Fig. 1G**). Together with the distinct expression of
158 cytotoxic markers, data suggests Tfh1 cells exist in two distinct and functionally relevant subests.

159 To dissect the relationship between the diversity of Tfh cells identified transcriptional, and the
160 phenotypic subsets these cells would have been characterized as with flow cytometry, the degree of
161 overlap between designated Tfh cell subsets and sorted cell phenotypes was analysed. Tfh1_cytotoxic,
162 Tfh1_CCR7, Tfh2 and Tfh17 clusters, defined by transcriptional profiles, were mainly found in cells
163 expressing *PDCD1*. Further, *CXCR3* and *CCR6* expression overlapped with the pTfh1 and Tfh17
164 sorted populations, respectively, suggesting some overlap between transcriptional clusters and those
165 identified via CXCR3 and CCR6 expression (**Fig. 1C**). Nearly all cells found within both Tfh1
166 transcriptional clusters (Tfh1_cytotoxic and Tfh1_CCR7), were from the pTfh1 sorted cell population.
167 However, the sorted pTfh1 population also contained cells from all other transcriptional subsets.
168 Similarly, the phenotypic pTfh2 population was dominated by the Tfh2 transcriptional subset but also
169 contained cells with diverse transcriptional annotations (**Fig. 1F, Supplementary Fig. 1F**). This
170 pattern was also seen for the phenotypic pTfh17 population. The PD1- phenotypic cells contained
171 cells of all clusters, but were dominated by IFNI, stress, ribosomal and cluster 2 and cluster 3 cells.
172 Thus, while commonly used flow cytometry strategies do overlap with transcriptional diversity,
173 further phenotypic markers would be required to fully dissect Tfh cell subsets.

174 To understand the clonal sharing between clusters, TCR sequences were analysed. TCR sequences
175 with complete TRA/TRB genes were captured for 3,998 (55.6%) cells. Clones were defined by the
176 sharing of identical amino acid sequences. While the majority of TRA/TRB cells were singletons
177 (3839 clones), clonal expansion was detected in 159 cells across 57 clones ranging in size from 2 to

20 identical clones. Clonal expansion was detected particularly within the Tfh1_cytotoxic subset (**Supplementary Fig. 1H**). As expected, no clones were shared across individuals (**Supplementary Fig. 1I**) Within each clonotype, we examined the fate sharing clones to investigate if clones of the same family tend to share the same transcriptional subsets or were found across diverse Tfh phenotypes. 40/57 clonotypes (70.2%) were found in a single subset. Clonal sharing was evident between Tfh1_cytotoxic and Tfh1_CCR7 but not Tfh2 transcriptional clusters, while Tfh2 shared clones with ribosomal, cluster 2 and cluster 3 cells (**Fig. 1G**). Together, these data show that while commonly used phenotypic markers CXCR3 and CCR6 can resolve some heterogeneity in pTfh cells, alternative distinct Tfh subsets, particularly within the pTfh1 compartment require additional phenotypic markers to dissect subsets of potential functional relevance.

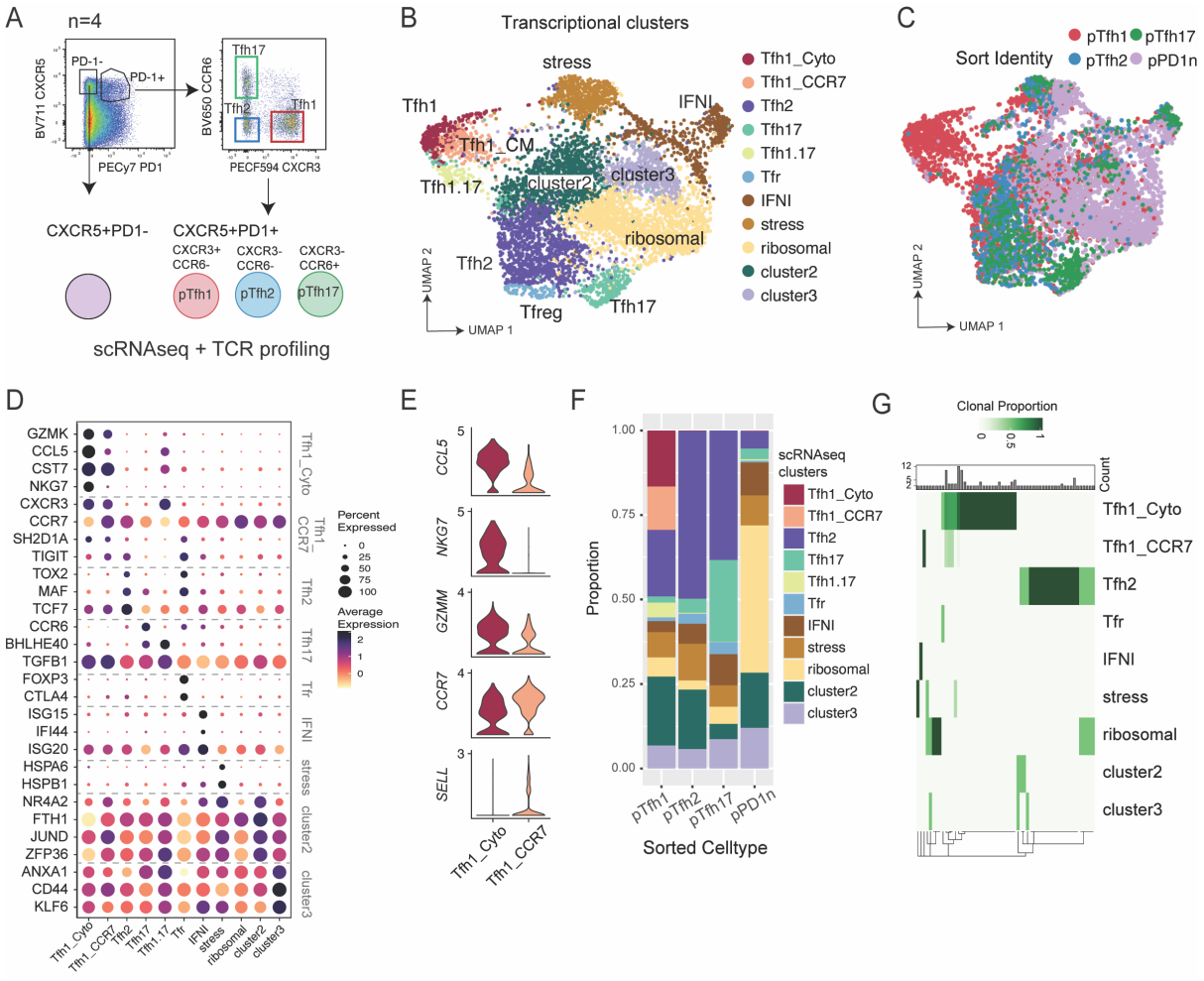

Fig. 1. scRNAseq analysis of pTfh cells from healthy individuals

*A. Four populations were sorted from pTfh CD4+ cells from 4 healthy donors - 1) CXCR5+PD1-, 2) CXCR5+PD1+ pTfh1, 3) CXCR5+PD1+ pTfh2, and 4) CXCR5+PD1+ pTfh17. Populations were analysed by 5' droplet scRNAseq for gene expression and TCR sequence. **B.** UMAP of data following integration by donor, with 11 transcriptional subsets indicated. **C.** UMAP of data depicting cell sorted identity. **D.** Relative gene expression of genes used to annotate transcriptional clusters. **E.** Average expression of key genes in Tfh1_Cyto and Tfh1_CCR7 annotated transcriptional clusters. **F.** Relationship between cell sorted identity and transcriptional cluster identity in the data set. **G.** Fate sharing at the individual clonotype level across transcriptional subsets. Expanded clonotypes ($n^3 2$) with only same fates (exist within the same subset), or different fates are shown See also Supplementary Fig. 1 and Supplementary Table S1 and S2.*

pTfh1 subsets with distinct phenotypic and functional characteristics can be defined by CCR7 expression

Transcriptional analysis identified two pTfh1-like subsets with distinct expression of cytotoxic and memory associated genes suggesting functional relevance. To assess if these subsets could be identified phenotypically and develop an approach to identify these subsets along with pTfh2 and pTfh17 cells in clinical cohorts, we designed a comprehensive phenotyping panel for pTfh cells which included commonly assessed chemokine receptors (CXCR3 and CCR6), markers identified in our transcriptional data set or with reported roles in Tfh cell function or development (**Supplementary Table S3)**. To test this approach to define Tfh subsets, we first analysed pTfh cells in healthy human donors (n= 19, sex 83.3% males, aged 24 years [20.2-28.2, median [IQR] years). pTfh cells were identified based on CXCR5 and PD1 expression, and then analysed with unsupervised clustering considering CXCR3, CCR6, CCR7, NKG7, GrzmB, GrzmK, cMAF, TIGIT and FoxP3. As seen in transcriptomic analysis, unbiased clustering consistently identified two subsets of pTfh1 cells based on CCR7 expression, where $CCR7^{neg}$ cells also expressed high levels of NKG7, GrzmB and GrzmK, while $CCR7^{pos}$ cells were negative for these markers (**Fig. 2A, Supplementary Fig. 2A-C).** pTfh2, pTfh17 and pTfh1-17 cells could also be identified with unbiased clustering (**Fig. 2A**). Additionally, FoxP3+ Tfr cells were identified and largely clustered within the pTfh2 cell subset, consistent with scRNAseq data (**Fig. 2A, Supplementary Fig. 2A-C**).

To assess if analysis of a single marker, CCR7, together with CXCR3 and CCR6 could capture this underlying diversity in Tfh1 cells, we next applied manual gating approaches. Within pTfh cells (CXCR5+PD1+ [FoxP3-/CD25-] CD4 T cells) a gradient of CCR7 expression was detected, and

223 pTfh1 cells could be divided into CCR7^{pos} and CCR7^{neg} subsets (**Fig. 2B, Supplementary Fig. 2D**).
224 Within pTfh subsets, expression of cytotoxic markers NKG7, GrzmB and GrzmK was significantly
225 higher in CCR7^{neg} pTfh1 compared to either CCR7^{pos} pTfh1 or pTfh2 and pTfh17 cells (**Fig. 2C-E**
226 **Supplementary Fig. 2E**). Within pTfh cells, we also quantified cMaf which was upregulated in Tfh2
227 cell clusters, and SAP (*SH2D1A)* and TIGIT which were increased transcriptionally in Tfh1_CCR7
228 cells (**Fig. 1D**). cMaf and SAP have essential roles in GC Tfh cell development [34], and TIGIT is
229 reported to have highest expression in GC-Tfh and pTfh2 cells [8]. cMaf expression was not different
230 between pTfh1 CCR7$^{neg/pos}$ cells, both of which had significantly lower expression compared pTfh2
231 and pTfh17, consistent with previous reports [8] (**Fig. 2F**). SAP expression was low across all subsets,
232 and was lowest in pTfh2, and comparable between the two pTfh1 subsets (**Fig. 2G**). Further, in
233 contrast to previous reports, TIGIT expression was highest on pTfh1 CCR7^{neg} cells compared to both
234 pTfh1 CCR7^{pos} and pTfh2 cells (**Fig. 2H**). Thus, while CCR7 expression could differentiate
235 populations of pTfh1 cells with distinct cytotoxic potential, how key transcriptional factors may
236 influence pTfh subsets requires further investigation.

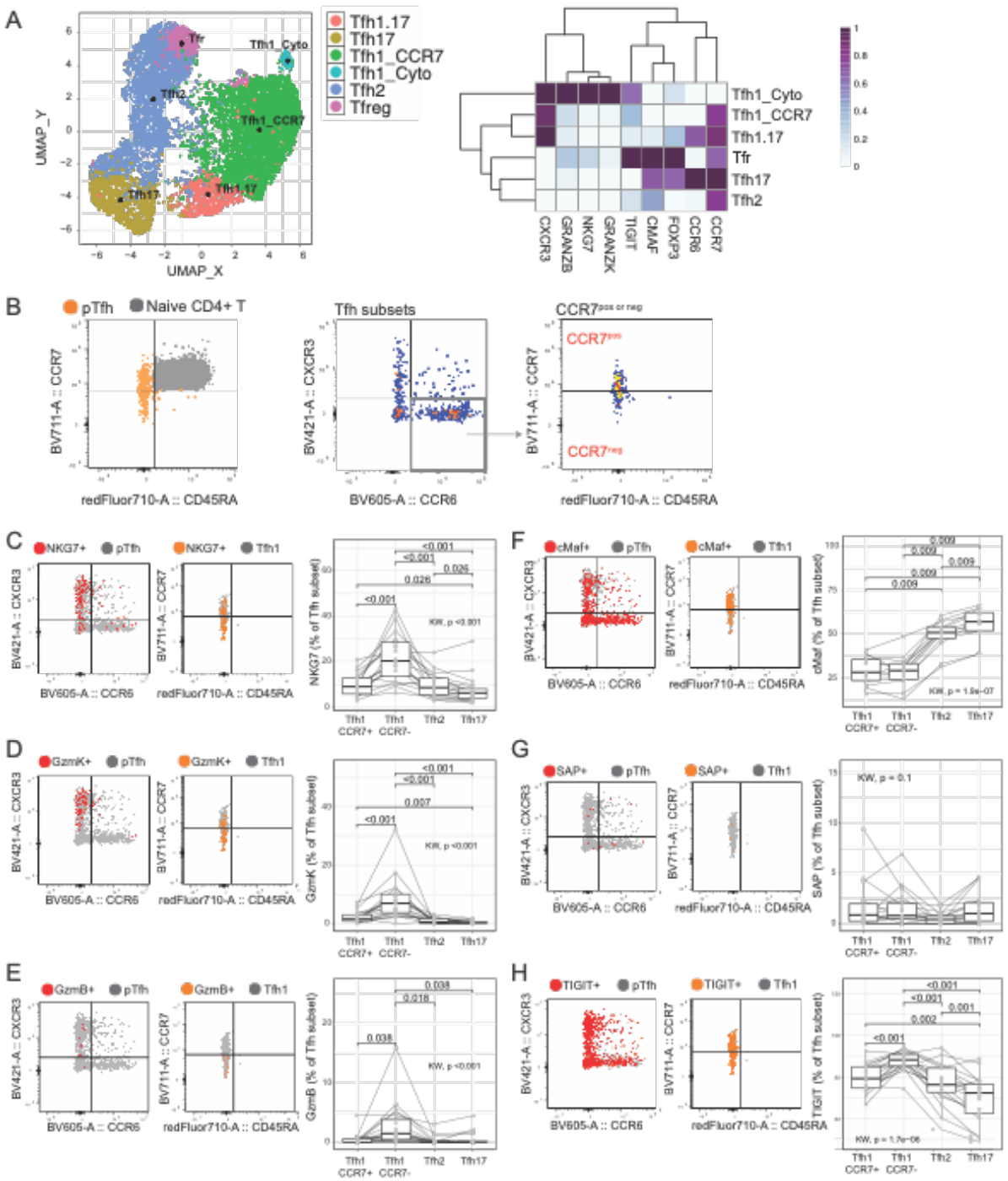

Figure 2: Phenotypic diversity of pTfh cell subsets based on CCR7 expression.
*A comprehensive spectral flow cytometry panel was used to analyse pTfh cells in healthy individuals (n =19). (**A**) pTfh cells were identified by CXCR5 and PD1 and analysed with unbiased analysis of indicated markers. UMAP of a single experiment analysing n=7 individuals. Analysis performed three independent times. (**B**) Tfh cells were analysed with manual gating. A gradient of CCR7 expression is detected within pTfh cells, and pTfh1 CCR7neg (CCR7-) and pTfh1 CCR7pos (CCR7+) subsets can be identified, along with pTfh2 and pTfh17 cells. Expression of cytotoxic markers NKG7 (**C**), Granzyme K (**D**) and Granzyme B (**E**) and transcriptional factors cMaf (**F**), SAP (**G**), and TIGIT (**H**) were analysed within pTfh cell subsets. Flow plots are a representative individual with marker expression overlayed against CXCR3 and CCR6 or CCR7 and CD45RA. Boxplots with median and IQR are indicated along with individuals. P is the paired Wilcoxon signed-rank test after adjustment*

249 *with multiple testing correction using Holm's method, while the Kruskal-Wallis test is used for the*
250 *global comparison. Only significant differences (p<0.05) are shown. See also Supplementary Fig. 2.*
251

252 To further investigate potential functional differences of pTfh1 cell subsets, cytokine production from
253 pTfh cells was quantified following PMA/Io stimulation in healthy donors (**Supplementary Fig. 3,**
254 **Supplementary Table S4,** n=11, sex 36.36 % males, age 37.5[32-40], median[IQR] years). As seen
255 *ex vivo*, a gradient of CCR7 expression is detected within pTfh1 cell subsets identified with CXCR3
256 and CCR6 expression post stimulation (**Supplementary Fig. 3A/B**). Following PMA/Io stimulation
257 and within the commonly identified pTfh1, pTfh2 and pTfh17 cell subsets, the production of the Tfh-
258 related cytokine IL-21 was comparable, while pTfh1 produced higher IFNγ and TNF, pTfh2 produced
259 higher IL-4 and pTfh17 produced higher IL-17, as expected (**Supplementary Fig. 3C/D**). Production
260 of the regulatory cytokine IL-10 was detected at low levels in all subsets. When pTfh1 cells were
261 analysed based on CCR7 expression, there was no difference between pTfh1 $CCR7^{pos}$ and CCR7neg
262 cells in IL-21, or TNF production, however Tfh1 CCR7neg cells produced significantly higher IFNγ,
263 IL-4 and a trend towards increased IL-10 (**Fig. 3A**). Further, when the total cytokine composition was
264 analysed, there was a significant difference in the cytokine composition produced by pTfh1 $CCR7^{pos}$
265 compared to $CCR7^{neg}$ cells (**Fig. 3B).** Given the importance of the milieu Tfh cytokine production in
266 B cell responses [5], data suggest that subsets may have nuanced roles in antibody induction during
267 infection.

268 Together, these data show that transcriptionally, phenotypically and functionally, pTfh1 cell subsets
269 identified by CXCR3+ expression can be further distinguished based on CCR7 expression. These data
270 highlight a previously unrecognised diversity of pTfh cells in healthy individuals when only
271 considering subsets identified by CXCR3 and CCR6 expression, which may have important
272 implication to B cell development during infection.

273

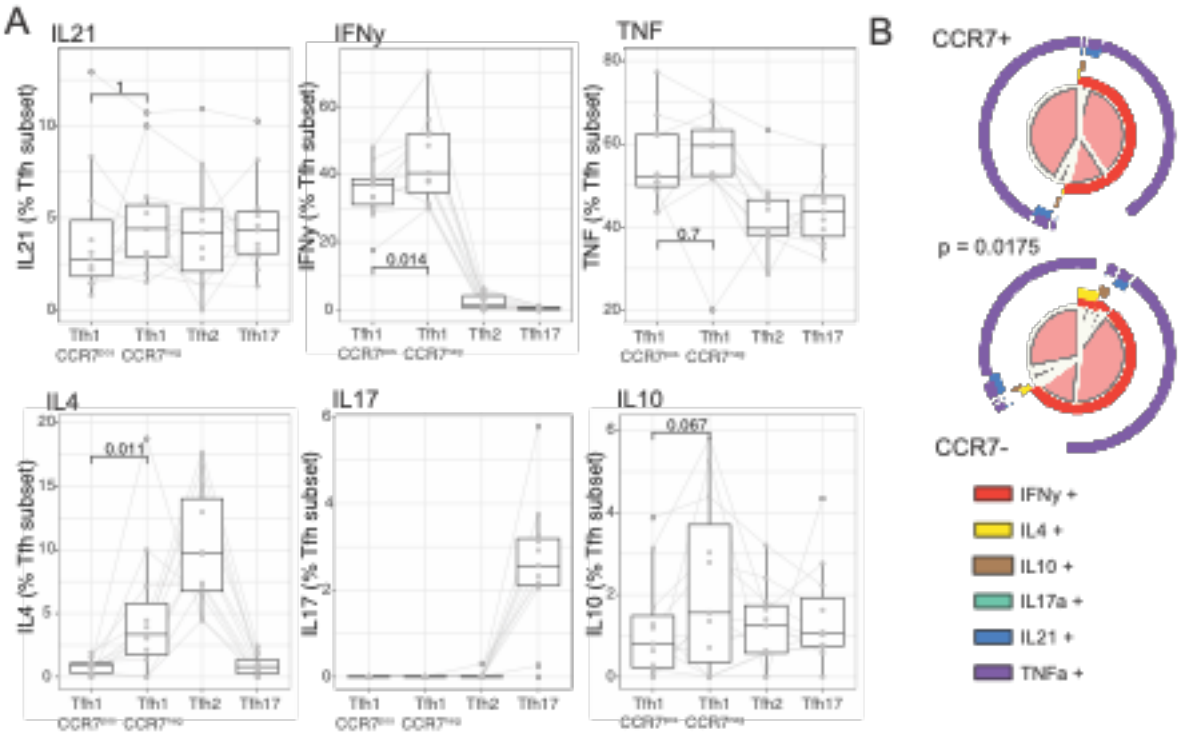

Figure 3. Functional diversity within pTfh cell subsets based on CCR7 expression
Cytokine production following PMA/ Io stimulation was measured by intracellular staining in healthy individuals (n=11). pTfh cells subsets were identified by CXCR3 and CCR6 expression as pTfh1 (CXCR3+CCR6+), pTfh2 (CXCR3-CCR6-) and pTfh17 (CXCR3-CCR6+), and pTfh1 cells subsets identified as CCR7^{pos} and CCR7^{neg} cells. ***A)****. IL-21, IFNγ, TNF, IL-4, IL-17, and IL-10 expression within pTfh cell subsets. P is the paired Wilcoxon signed-rank test between pTfh1 cell subsets.* ***B)*** *Overall cytokine production within pTfh1 CCR7^{pos} and CCR7^{neg} cells. P is permutation test in SPICE. Box and whisker plots indicate first and third quartiles for hinges, median line and lowest and highest values no further than 1.5 IQR from hinges. All individual data are represented by the grey dots and lines. See also Supplementary Fig. 3.*

Expansion of pTfh1 and pTfh2 cell subsets in human malaria infection

To investigate the roles of pTfh1 CCR7^{pos} and pTfh1 CCR7^{neg} subsets, along with other pTfh cells, during infection, we applied findings to human malaria with samples from a CHMI study cohort. pTfh cells (CD45RA-CXCR5+PD1+) were sorted from individuals in CHMI at day 0 (prior to inoculation), day 8 (peak infection), day 15 and day 36 (both after anti-parasitic drug treatment), and their transcriptional profiles analysed using 5' droplet scRNAseq (n =4, 100 % males, age 22 [21.5-26], median [IQR] years, **Supplementary Fig. 4A/B**). After QC, 27,552 cells were analysed, with high quality cells captured from each donor and timepoint (day 0 n = 6,741, day 8 n=6,125, day 16 n=8,103, day 36 n=7,583, **Supplementary Fig. 4C**). Data were integrated based on donor and time point **(Supplementary Fig. 4D),** and pTfh cell clusters identified by label transfer with scType (an

296 automated cell-type identification tool [35]), using the top 20 upregulated and downregulated marker
297 genes for each cell cluster identified in the healthy 'map' data set used as a reference
298 (**Supplementary Table S5**, **Supplementary Fig. 4E-H**). scType specificity scores were used to
299 collapse clusters into cell subsets (**Figure 4A, Supplementary Fig. 4H**). This approach identified
300 Tfh1_cytotoxic, Th1_CCR7, Tfh2, Tfh17, IFNI, stress, ribosomal, cluster 2 and cluster 3 subsets.
301 Tfh1.17 and Tfr cells were not included in the reference map because of overlapping signatures with
302 Tfh1/Tfh17 and Tfh2 subsets. Following label transfer, Tfh1.17 could not be identified manually,
303 however Tfr cells were identified by inspection of marker genes *FOXP3, CTLA4* and *IL2RA* (**Fig.**
304 **4B**). Gene expression of annotated cell clusters was consistent with the reference data set (**Fig. 4B,**
305 **Supplementary Fig. 4G, Supplementary Table S6**). For example, Tfh1_cytotoxic and Tfh1_CCR7
306 clusters both expressed *CXCR3*, with the two clusters having differing levels of inflammatory markers
307 including *GZMK*, *CCL5* and *NKG7,* which were increased in Tfh1_cytotoxic, and the memory
308 markers *SELL* and *CCR7,* which were increased in Tfh1_CCR7 (**Fig. 4B)**. Similarly, Tfh17 cells
309 identified with label transfer had increased expression of *CCR6*, *BHLHE40* and *TNFRSF4*.
310 Interestingly, *TCF7*, *MAF* and *TOX2*, which were identified as marker genes in the reference data set
311 for Tfh2, were expressed both within the Tfh2 subset, but also relatively increased in the Tfh1_CCR7
312 cells in the infection data set (**Fig. 4B, Supplementary Fig. 4G).** Together, these data show the utility
313 of the reference map data set to identify Tfh cell subsets within sorted pTfh cells during multiple time
314 points in infection.

315 To investigate how the Tfh cell compartment was impacted by malaria, we assessed the proportion of
316 each cluster over time. There was a clear expansion of the Tfh1_CCR7 subset in all individuals at day
317 16 post infection, while Tfh1_cytotoxic cells were expanded at this time point to a lesser magnitude
318 (**Fig. 4C**). Tfh2 cells expanded in three of four individuals at day 8, consistent with the earlier
319 activation of this subset in this cohort reported previously [12]. Other subsets were not clearly impacted
320 by infection (**Supplementary Fig. 4I)**. Within each subset, TCRA/B sequences were analysed. TCR
321 sequences with complete TRA/TRB genes were captured for 21,939 (77.97%) cells, and this was
322 comparable across the days/cell types (**Supplementary Fig. 5A**). Clones were defined as cells sharing

323 identical amino acid sequence in both TRA and TRB. During CHMI there was evidence of clonal
324 expansion at day 16, with a significant increase in clonal family size greater than 1 (**Fig. 4D/E**), and
325 increased Simpson Index, indicating increased clonal expansion (**Fig. 4F**). Expansion was highest in
326 Tfh1_cytotoxic and Tfh1_CCR7 clusters, consistent with the increased frequency of these cells and
327 indicative of clonal proliferation (**Fig. 4E, Supplementary Fig. 5B**). Clonal expansion was also
328 detected within Tfh2 cells at day 16 (**Fig. 4E**). As expected, minimal clonal sharing was detected
329 between donors with only a single clone shared between donor 0 and donor 1 on day 36, which may
330 indicate sequence convergence detected due to analysis of clones with amino acid rather than
331 nucleotide sequence [36,37] (**Supplementary Fig. 5C**). All other clonal sharing occurred within an
332 individual, the majority at a single timepoint (**Supplementary Fig. 5D**). For donor 3, clones were also
333 shared across time points including day 0 prior to malaria, with large clonal families maintaining a
334 single fate across time in the Tfh1_cytotoxic cell cluster, possibly indicating a subset expansion
335 during a prior infection (**Supplementary Fig. 5D**). At day 16, where malaria associated expansion
336 was most evident, clonal sharing across Tfh cell clusters were analysed. While there was a minimal
337 sharing between Tfh1_cytotoxic and Tfh2 cell subsets, Tfh1_CCR7 cells shared clones with both
338 Tfh1_cytotoxic and Tfh2 cells, consistent with the overlapping profiles of Tfh1_CCR7 with both
339 Tfh1_cytotoxic and Tfh2 subsets (**Fig. 4G**). Taken together, these data are consistent with the
340 emergence of malaria specific Tfh cells with diverse transcriptional signatures during infection. These
341 include pTfh1 $CCR7^{pos}$ cells with increased functional capacity, pTfh1 $CCR7^{neg}$ cells with cytotoxic
342 phenotypes, and pTfh2 cells which are transcriptionally most similar to GC Tfh cells [8].

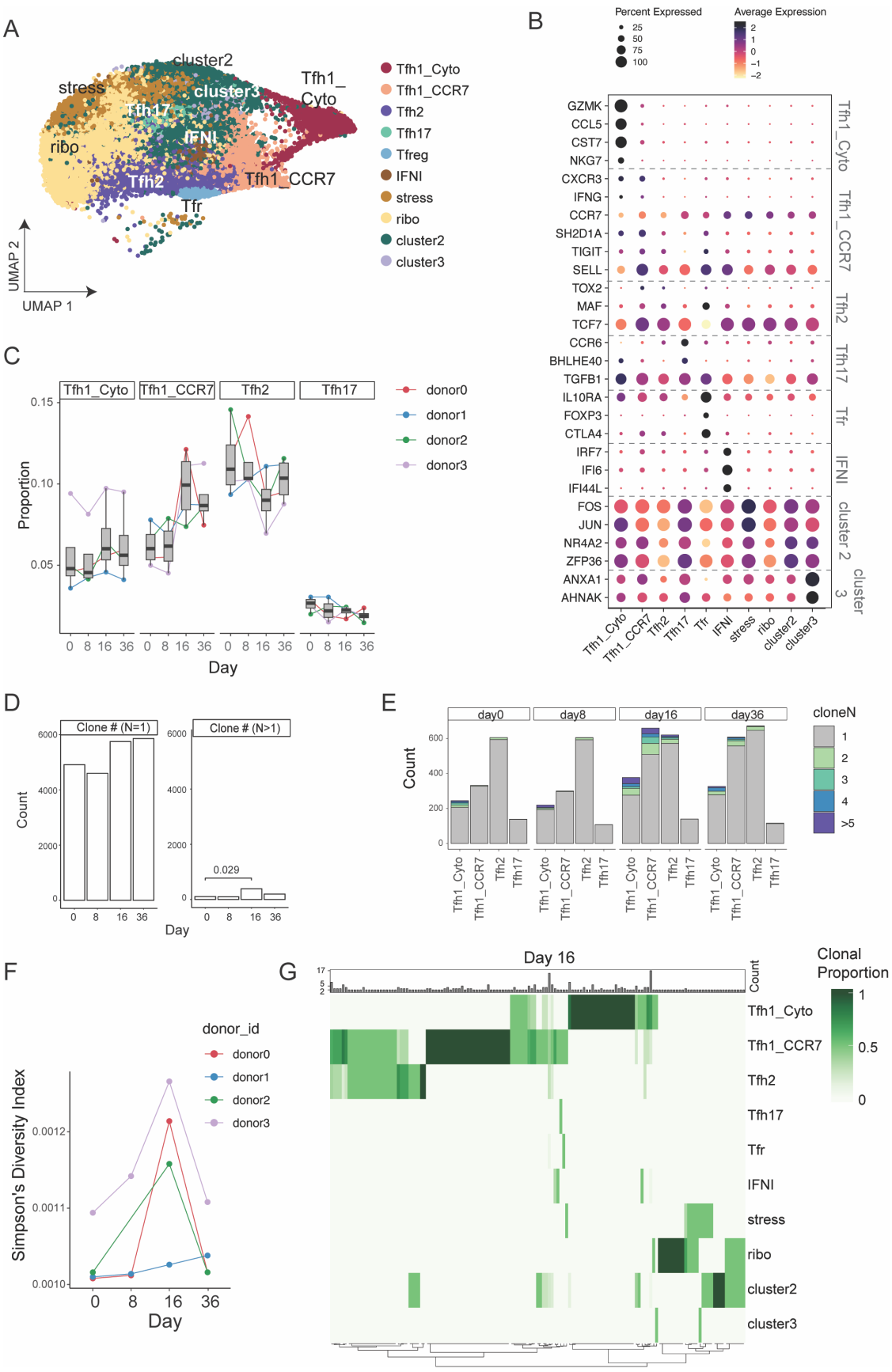

343

344 ***Figure 4: Clonal expansion of diverse pTfh cell subsets during malaria infection***

345 *A) pTfh cells (CXCR5+PD1+nnCD4 T cells) were isolated from individuals (n=4) during controlled*
346 *human malaria infection (CHMI) at day 0, 8, 16 and 36. scType label transfer was used to identify Tfh*
347 *transcriptional subsets using the healthy Tfh cell data set as a reference.* ***B.*** *Average expression of*
348 *marker genes used to annotate reference data set in each subset in CHMI data set* ***C.*** *Relative*
349 *proportion of each pTfh transcriptional cluster during CHMI. Each individual is show. Statistical*
350 *testing was not performed due to limited sample size in scRNAseq data set.* ***D.*** *Counts of clones with*
351 *either a clone size = 1 (top) or clone size ≥ 2 across days (bottom). Clonal expansion was detected at*
352 *day 16.* ***E.*** *Clone family size count over time in each subset - Clonal expansion was detected in*
353 *Tfh1_cyto, Tfh1_CCR7 and Tfh2 clusters at day 16.* ***F.*** *Simpsons diversity Index in each donor across*
354 *time.* ***G.*** *Clonal overlap at day 16 across clusters. Clonal size is indicated in count in top bar, each*
355 *clonal proportion across subsets is indicated. See also Supplementary Fig. 4 and 5.*
356

357 **Unique transcriptional activation of Tfh1 subsets during human malaria infection**

358 To investigate transcriptional pathways activated in each Tfh transcriptional subset during malaria,
359 differential gene expression between day 0 and subsequent time points was performed with pseudo-
360 bulk analysis, grouped by individual (**Supplementary Table S7**). The largest transcriptional changes
361 were detected at day 16 within the Tfh1_CCR7 and Tfh1_cytotoxic subsets (**Fig. 5A**). Differentially
362 expressed genes (DEGs) at day 16 were also detected in Tfh2 cells consistent with clonal expansion
363 of these cells, and previously reported findings [12] (**Fig. 5A**). The number of DEGs was contracted by
364 day 36, with DEGs detected at this time point restricted to Tfh1_CCR7, suggesting this subset had a
365 sustained response to infection. The majority of DEGs at day 16 from Tfh1_CCR7, Tfh1_cytotoxic,
366 and Tfh2 were subset specific (**Fig. 5B**). Shared across all three subsets was the activation marker
367 *CD38*, and Tfh1_cytotoxic and Tfh1_CCR7 cells also both upregulated *MKI67* consistent with
368 proliferation and clonal expansion of these cells during malaria. However, overall expression of
369 activation and proliferation genes was highest in Tfh1_CCR7 cells (**Fig. 5C, Supplementary Fig.**
370 **6A**). Analysis of the top 20 upregulated genes from Tfh1_CCR7, Tfh1_cytotoxic and Tfh2 cells
371 highlighted the uniquely upregulated gene signatures identified from Tfh1_CCR7 and Tfh1_cytotoxic
372 cells (**Fig. 5D, Supplementary Fig. 6D**). Additionally, while shared upregulated genes also included
373 genes associated with increased inflammation and cytotoxicity including *NKG7, CCL5, GZMH,*
374 *CXCR3* and *IFNG* the level of these genes was significantly higher in Tfh1_cytotoxic cells (**Fig. 5D**,
375 **Supplementary Fig. 6B**). Further, the transcriptional profile of Tfh2 cells was also maintained and
376 similar to that seen at day 0, despite upregulation of Tfh1 associated genes (**Supplementary Fig. 6C**).

Taken together, scRNAseq analysis of pTfh cells during malaria identify the activation, proliferation and clonal expansion of Tfh1_CCR7, Tfh1_cytotoxic and Tfh2 cells with unique transcriptional activation profiles.

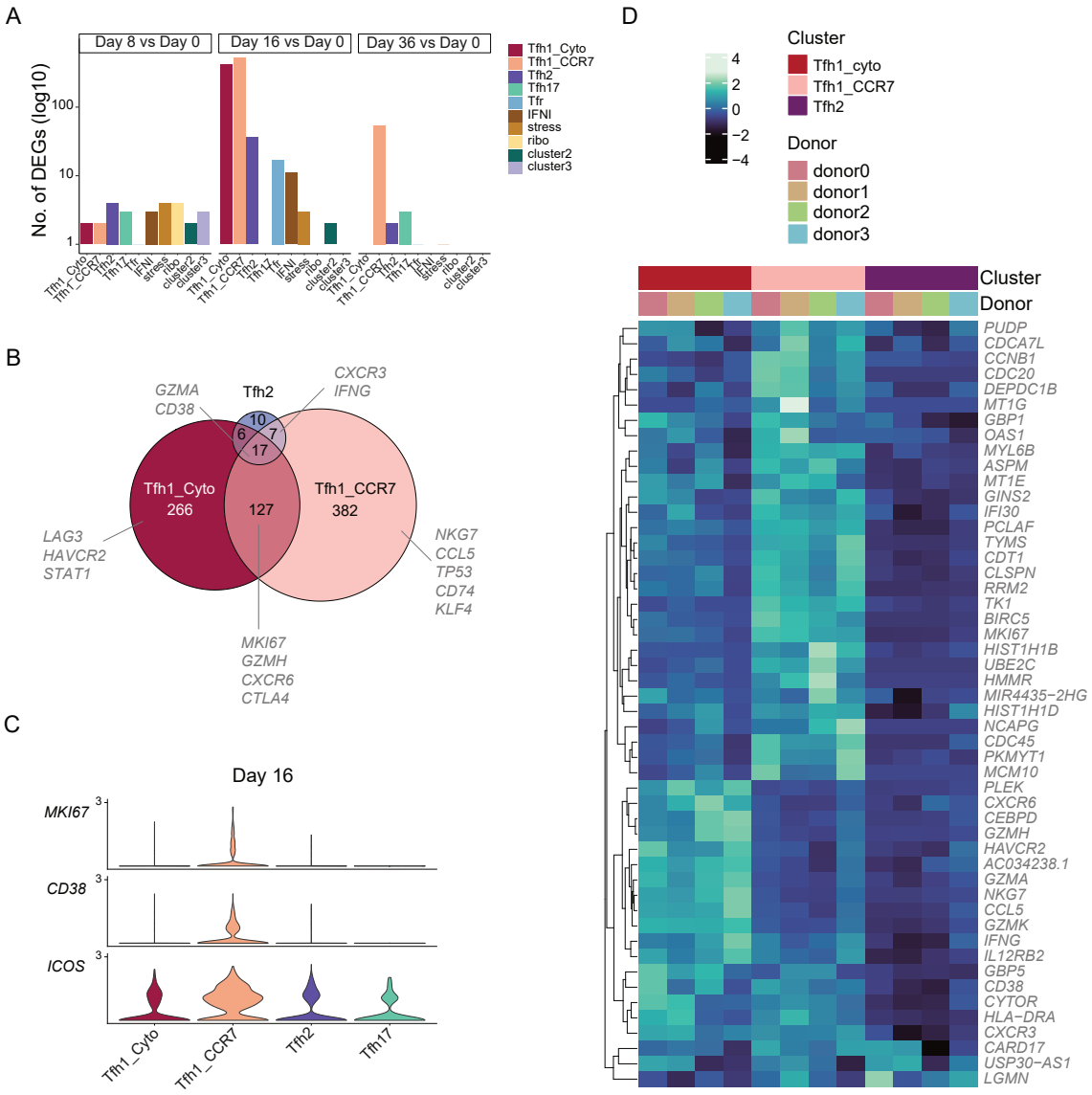

Figure 5: Transcriptional activation of Tfh cell subsets during controlled human malaria infection ***A.*** *DEGs for each cluster were calculated at day 8, 16, and 36 compared to day 0. The number of DEGs for each subset and timepoint.* ***B.*** *Venn diagram indicating the shared and unique DEGS at day 16 for Tfh1_cytotoxic, Tfh1_CCR7 and Tfh2 subsets.* ***C.*** *Average expression of activation genes MKI67, CD38 and ICOS at day 16 in each Tfh subset compared to Day 0.* ***D.*** *Average expression of top 50 unique upregulated genes for Tfh1_Cyto, Tfh1_CCR7 and Tfh2 (curated from top 20 upregulated DEGs in Tfh1_CCR7, Tfh1_cytotoxic and Tfh2) cells across all three subsets at day 16 subsets. See also Supplementary Figure 6.*

390 **Frequency and proliferation of malaria specific pTfh CCR7^{pos} cells is associated with the**
391 **magnitude and function of antibody induction in CHMI**

392 To confirm transcriptional findings at the phenotypic and antigen specific level and assess
393 associations of different pTfh subsets with antibody induction, we applied our flow cytometry panel to
394 identify pTfh subsets, including pTfh1 CCR7^{pos} and CCR7^{neg} cells to assessed the activation of pTfh
395 cells during CHMI in a subset of individuals from a previously published cohort (n= 19, sex 83.3%%
396 males, aged 24 years [20.2-28.2, median [IQR] years) [12]. Here we expanded on the published analysis
397 by focusing on malaria specific pTfh cells which were identified by Activated Induced Marker (AIM)
398 assays following PBMC stimulation with parasite infected RBCs (pRBCs) [16] (**Supplementary Fig.**
399 **7A).** Consistent with scRNAseq analysis, AIM+ (CD69+OX40+) pTfh cells were expanded at day 16
400 and 36 during CHMI. The frequencies of cells detected in control stimulated cultures (uninfected
401 RBCs) were unchanged (**Fig. 6A).** The largest response of malaria specific (AIM+ in pRBC stim)
402 pTfh cells occurred in pTfh1 CCR7^{pos} cells, however, increased frequencies of Tfh1 CCR7^{neg} and
403 Tfh2 cells were also detected, consistent with the proliferation and expansion of these cells detected
404 transcriptionally (**Fig. 6B**). Proliferation of AIM+ pTfh17 cells were also detected at day 36
405 (p=0.051), however given that pTfh17 cells did not expand clonally, nor have any detectable
406 transcriptional changes during infection, these cells are likely to be TCR independent cells which are
407 activated via cytokines within AIM assays [38]. Within malaria specific pTfh1 CCR7^{pos}, pTfh1 CCR7^{neg}
408 and pTfh2 cells, there were significant increases in expression of activation markers ICOS and CD38,
409 and proliferation marker Ki67 at day 16 and 36 (**Fig. 6C/D**). However, the expression of these
410 markers was significantly higher on malaria specific pTfh1 CCR7^{pos} cells compared to other subsets,
411 consistent with the greatest expansion and activation of pTfh1 CCR7^{pos} cells transcriptionally (**Fig.**
412 **6E/F**).

413 To investigate the link between each malaria specific pTfh cells and antibody development, we
414 correlated malaria-specific pTfh cells with antibodies produced after infection in response to intact
415 merozoites, quantified previously [12]. Antibody development was quantified with an antibody score
416 which captured the magnitude, breadth and functionality of response, by measuring IgM, IgG and IgG

417 subclasses, C1q fixation, FcR crosslinking and opsonic phagocytosis [12]. The frequencies of malaria-
418 specific pTfh1 CCR7^{pos}, pTfh1 CCR7^{neg} and pTfh2 cells correlated with each other, but not with
419 pTfh17 cells (**Fig. 6G)**. Despite this, pTfh1 CCR7^{pos} were correlated the most strongly and
420 consistently with antibody induction compared to other subsets, and were positively correlated with
421 total antibody score, and IgM and IgG to the merozoite (**Fig. 6G**), along with IgG1 and IgG2
422 (**Supplementary Fig. S7B).** In contrast, pTfh1 CCR7^{neg} cells only correlated with IgM and pTfh2
423 cells only correlated with antibody score (**Fig. 6G**). Similarly, while Ki67 expression amongst subsets
424 was correlated, only Ki67+ pTfh1 CCR7^{pos} and Ki67+ pTfh2 cells were correlated with antibody
425 score, IgG and IgM and antibody functions (**Fig. 6H, Supplementary Fig. S7D/E)**. Together, data
426 highlight that pTfh1 CCR7^{pos} and pTfh1 CCR7^{neg} cells have distinct functional potential. While both
427 are activated in malaria, pTfh1 CCR7^{pos} cells, together with pTfh2 cells, are more strongly associated
428 with antibody development.

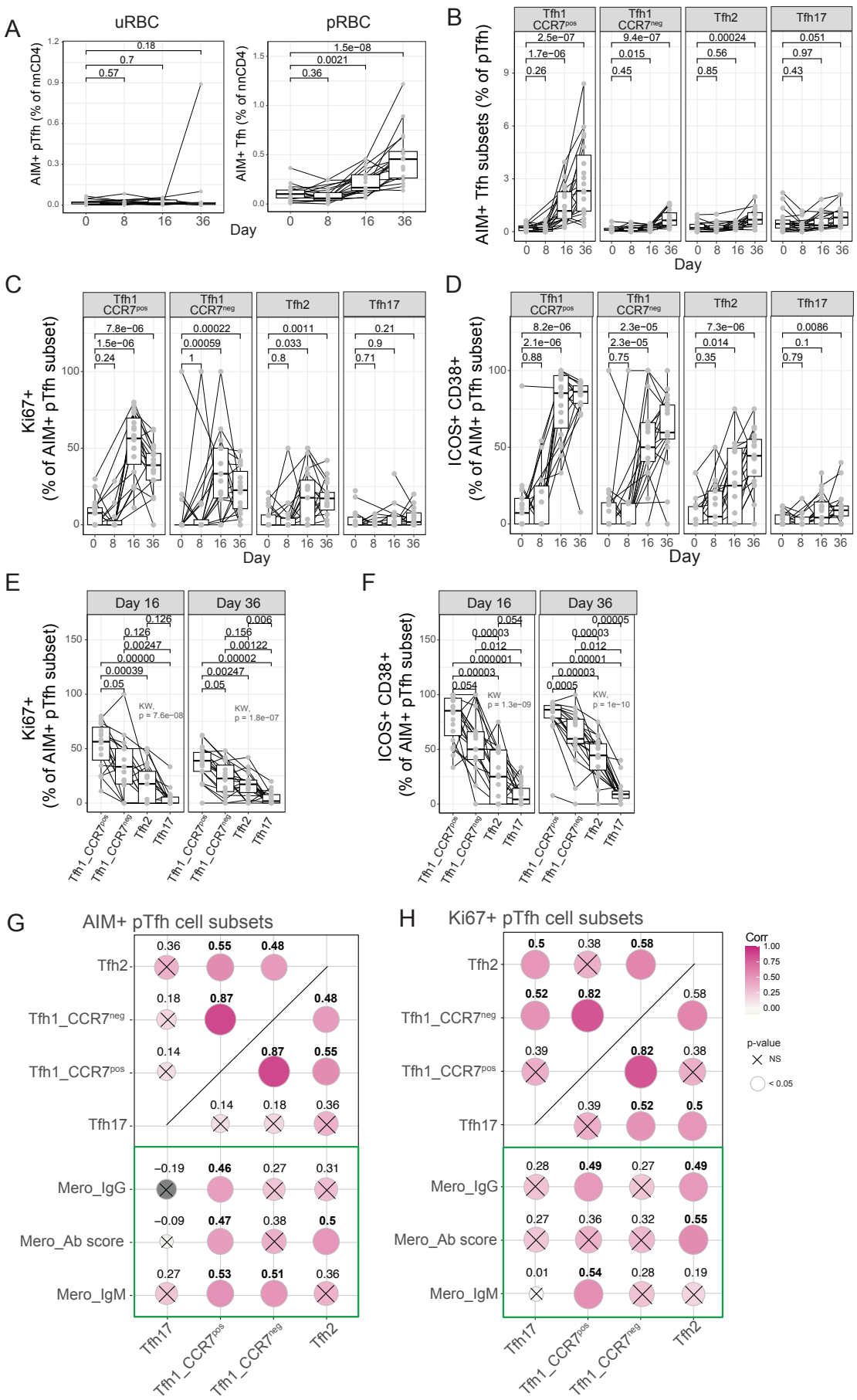
A
uRBC
pRBC
AIM+ pTfh (% of nnCD4)
AIM+ Tfh (% of nnCD4)
Day
B
Tfh1 CCR7pos
Tfh1 CCR7neg
Tfh2
Tfh17
AIM+ Tfh subsets (% of pTfh)
Day
C
Ki67+ (% of AIM+ pTfh subset)
Day
D
ICOS+ CD38+ (% of AIM+ pTfh subset)
Day
E
Day 16
Day 36
Ki67+ (% of AIM+ pTfh subset)
KW, p = 7.6e−08
KW, p = 1.8e−07
F
ICOS+ CD38+ (% of AIM+ pTfh subset)
KW p = 1.3e−09
KW, p = 1e−10
G
AIM+ pTfh cell subsets
Tfh2
Tfh1_CCR7neg
Tfh1_CCR7pos
Tfh17
Mero_IgG
Mero_Ab score
Mero_IgM
H
Ki67+ pTfh cell subsets
Corr
p-value
NS
< 0.05

429

Figure 6: Activation of malaria specific Tfh cells during malaria infection and association with antibody induction

A. *Activation induced marker (AIM) assays were used to detected malaria specific pTfh cells in individuals following CHMI (n= 15-20). AIM+ cells were identified as CD69+OX40+ pTfh cells after stimulation with uninfected or parasite infected RBCs (uRBC and pRBC respectively) within all non-naïve CD4 T cells. Malaria specific Tfh cells increased at day 16 and day 36 after infection.* ***B.*** *Malaria specific (AIM+) subset specific pTfh cells as a proportion of total pTfh cells.* ***C-D.*** *Ki67+ (C) and ICOS+CD38+ (D) cells as a percentage of each AIM+ malaria specific pTfh subset during CHMI comparing changes with infection.* ***E-F.*** *Ki67+ (E) and ICOS+CD38+ (F) cells as a percentage of each AIM+ malaria specific pTfh subset at day 16, comparing expression levels between subsets.* ***G-H.*** *Correlation between (**G**) malaria specific pTfh cell subsets or (**H**) Ki67 expression of Tfh subsets at day 36 with total IgG and IgM levels to merozoite, and overall antibody score against merozoite, which captures the total antibody magnitude, breadth and functionality specific to merozoite.* ***A-D****. P is the Wilcoxon rank-sum test for each infection timepoint against baseline.* ***E-F****. P is the Wilcoxon rank-sum test after adjustment with multiple testing correction using Holm's method, while the Kruskal-Wallis test is used for the global comparison.* ***G-H****. Spearman's rho and p-value are indicated. See also Supplementary Figure 6 and Supplementary Figure 7.*

Discussion

Here we provide data that advances understanding of Tfh cell subsets, highlighting their functional diversity across the course of human malaria. Using unbiased analysis to integrate pTfh in the resting state, we identify two clearly distinct pTfh1 subsets, which we show can be distinguished based on CCR7 expression phenotypically. pTfh1 CCR7^{pos}cells do not express cytotoxic markers and produce less inflammatory cytokines, but similar IL-21 levels compared to pTfh1 CCR7^{neg} cells. Expanding our findings to the context of human infection, we show during malaria that while pTfh1 CCR7^{pos}, pTfh1 cytotoxic/CCR7^{neg}, and Tfh2 cell subsets expand, and are activated, activation pathways are unique between the subsets. We show both transcriptionally and at the malaria specific level, the magnitude of activation is greatest in pTfh1 CCR7^{pos} cells, which also expand clonally. Additionally, the frequency and proliferation of pTfh1 CCR7^{pos} cells was most consistently associated with antibody induction compared to other subsets. Taken together, these findings provide new knowledge on Tfh cell activation and functions during human infection. The specific role of pTfh1 CCR7^{pos} and pTfh2 cells, but not pTfh1 CCR7^{neg} responses in antibody induction during malaria informs approaches to target Tfh cells to improve antibody development and protection.

Understanding the mechanisms driving the development of distinct Tfh cell subsets has important translational implications for vaccine design and therapeutic interventions. Development of distinct

465 Tfh cell subsets is suggested to be mediated by cytokine skewing driven by distinct inflammatory
466 milieu occurring during different immune responses to infection or vaccination [5]. A recent
467 investigation of Tfh cell development in mice immunized with Type-1 or Type-2 adjuvanted
468 conditions supported this concept, inducing Tfh1 or Tfh2 cell-dominated responses, respectively [32].
469 However, a comparative investigation of Tfh cell development and function in different infections has
470 highlighted that cytokine signalling within Tfh cells is more important in driving subset fate than
471 pathogen class [7]. For example, within that study Tfh cell fates induced by LCMV and influenza, both
472 of which drive type-1 immune responses, were distinct and drove differing antibody responses [7],
473 highlighting nuanced roles of Tfh cell subsets in pathogen specific antibody development. While Tfh
474 cells enriched for different cytokine signalling pathways could be identified in human tonsils [7], how
475 distinct Tfh cell subsets develop in human infection is unclear. Further, our data highlight that even
476 within a single infection, induced pTfh cells are diverse. During malaria infection both pTfh1 CCR7^{pos}
477 and CCR7^{neg} subsets, along with pTfh2 are expanded, transcriptionally activated and malaria specific.
478 pTfh1 CCR7^{pos} cells shared clonal overlap with both pTfh1 CCR7^{neg} cells and pTfh2 subsets, but
479 these later subsets were largely clonally distinct from each other. Shared clonal relationships of
480 malaria specific pTfh1 and pTfh2 cells has been reported previously [39]. Whether these relationships
481 indicate cells along a single developmental pathway, or divergence from a parent population and how
482 cytokine signalling may influence subsets development is unknown.

483 The importance of understanding Tfh cell subset development is highlighted by the distinct functional
484 consequences on antibody development linked to Tfh cell subset function. Human studies linking Tfh
485 cell subsets to antibody development have largely been limited to identifying Tfh cell subsets based
486 on CXCR3 and CCR6 expression [8,9,40,41], including in malaria [12,16,17,19,39]. Alternatively, studies which
487 include a more comprehensive analysis of pTfh cells have not related Tfh cell diversity to antibody
488 development [31,42]. Here, our scRNAseq analysis shows that while CXCR3 and CCR6 are informative,
489 diversity is masked by this gating strategy. Of functional relevance, within pTfh1-like cells, we found
490 that pTfh1 CCR7^{neg} cells contain the large majority of Tfh cells expressing cytotoxic markers,
491 including *NKG7,* granzyme K and granzyme B. In contrast, these markers were absent from Tfh1

492 CCR7^{pos} cells, which produce less inflammatory cytokines but comparable levels of IL-21, resulting
493 in distinct cytokine milieu. Tfh cells with expression of cytotoxic markers have been identified
494 previously, and GC-Tfh cells which produce granzyme B in response to group A *Streptococcus* kill B
495 cells, potentially hampering antibody development [43]. More recently granzyme K+ CMV specific
496 pTfh cells were reported in humans. However, the function of these cells in the context of antibody
497 development is unknown [32]. During malaria infection, we show that that while malaria specific pTfh1
498 CCR7^{pos}, pTfh1 CCR7^{neg} and pTfh2 cell subsets are induced, only pTfh1 CCR7^{pos} and pTfh2 cell
499 subsets were clearly associated with antibody development. We have previously reported in the same
500 cohort that global pTfh2 cell activation early in infection (not considering antigen specificity) was
501 associated with antibody development [12]. While the importance of pTfh2 cells in antibody
502 development to malaria has been supported by others [13–15], a negative role of pTfh1 in antibody
503 development was difficult to rationalise in the context of what is known from *in vitro* studies and
504 animal models of induction of cytophilic IgG3 antibodies which protect from malaria [21]. Further, our
505 data from children in Ugandan in a high malaria transmission setting showed that children who had
506 the highest levels of functional antibodies had increased proliferating pTfh2 and pTfh1 cells [19]. Data
507 here resolve these contradictions with the identification of distinct pTfh1 cell subsets. Further studies
508 are required to investigate whether pTfh1 CCR7^{neg} cells with cytotoxic functions have negative roles
509 in antibody induction, and how pTfh1 CCR7^{pos} and pTfh2 cells function to induce protective
510 antibodies in malaria.

511 Limitations of our study include the analysis of pTfh cells isolated from peripheral blood of
512 volunteers, and not GC-Tfh within secondary lymphoid tissues. Future approaches to obtain and
513 analyse human secondary lymphoid tissue in the context of health and disease are needed. While pTfh
514 cells share overlapping signatures with GC-Tfh cells and are thought to provide a snapshot of the GC
515 response [6], activated pTfh may not fully represent all GC-Tfh phenotypes and functions [44]. Future
516 studies will focus on developing approaches for fine needle aspirate studies of draining lymph nodes
517 during human malaria infection as applied to COVID and influenza vaccination settings [44–48] , and
518 investigating the immune response within the spleen in malaria infected individuals which is likely a

519 key site of antibody development in blood stage malaria [49,50]. Nevertheless, such approaches are not
520 feasible for large human cohorts, thus data here on pTfh cells provides important insights that can be
521 applied to other human infection and vaccinations. Future studies dissecting mechanisms of protective
522 and disruptive Tfh cell development may lead to avenues to modulate Tfh cells during infection or
523 vaccination to induced more robust and protective antibody responses.

524 In conclusion, this study provides important new knowledge on functional diversity with pTfh cells
525 during human infection. We identify specific pTfh cell subsets that associate with antibody induction
526 in malaria, thus informing the development of approaches that can target these cells to improve
527 antibody development induced during vaccination. We provide a scRNAseq data set that can be
528 applied to other diseases, and a optimised approach to identify distinct pTfh1 subsets based on CCR7
529 expression. The identification of further Tfh subsets and their potential functional importance is
530 highly relevant to developing novel therapeutics or new vaccine strategies that can induce potent and
531 long-lasting immunity against not only malaria, but other important pathogens.

532

533 **Materials and methods**

534 **Ethics statement**

535 Ethics approval for the use of human samples was obtained from the QIMR Berghofer Human
536 Research Ethics Committee (HREC P1479) and the Alfred Health Ethics Committee (288/23).
537 Written informed consent was obtained from all study participants.

538 **Study cohorts**

539 For CHMI studies, inoculum preparation, volunteer recruitment, infection, monitoring and treatment
540 were performed as previously described [51]. In brief, healthy malaria naive individuals underwent
541 CHMI with 2800 viable *P. falciparum* parasitized RBCs, and peripheral parasitaemia was measured at
542 least daily by qPCR as described previously [52]. Participants were treated with antimalarial drugs at
543 day 8 of infection when parasitaemia reaches approximately 20,000 parasites/ml. Blood samples

544 (from 5 studies across 6 independent cohorts) were collected prior to infection (day 0), at peak
545 infection (day 8) and 14 or 15 and 27-36 days (end of study, EOS) after inoculation (in analyses these
546 time points are grouped as 0, 8, 14/15 and EOS). PBMCs were isolated by Ficoll-Paque (Sigma,
547 USA) density gradient centrifugation, isolated PBMCs were cryopreserved in 10% DMSO/FBS.
548 Participants were healthy malaria naïve adults with no prior exposure to malaria or residence in
549 malaria-endemic regions. Clinical trials were registered at ClinicalTrials.gov NCT02867059 [53],
550 NCT02783833 [54], NCT02431637 [55], and NCT02431650 [55]. For trials NCT02867059,
551 NCT02783833, NCT02431637 all participants received the same study drug (no-randomization) and
552 3D7-strain parasites. For NCT02431650, participants were randomized 1:1 to receive study drug
553 or control and 3D7-strain parasites. Samples used here were from samples opportunistically
554 collected from volunteers who consented to donate blood for immunological studies within the parent
555 clinical trial. As such, no sample size estimation was performed for this immunology study.

556 PBMCs from healthy non-infected controls was collected by the same processes for analysis of
557 responses following PMA/Io stimulation, development of transcriptional map of pTfh cells in health
558 donors.

559 *Sex as a biological variable:* Both male and females were included in this study. For some parent
560 CHMI studies females of child baring age were excluded and as such the sex distribution is not evenly
561 distributed.

562 **Ex vivo cell phenotyping with flow cytometry and activation induced marker assays**

563 PBMCs were thawed in RPMI 1640 (Gibco) containing 10% FCS and 0.02% Benzonase and rested
564 for 2 hours at 37°C, 5% CO2, and then cultured overnight in 96-well plates in 10% FCS/RPMI at 1 x
565 10^6 cells per well and stimulated for 18 hours with pRBCS or uninfected red blood cells (uRBCs) at
566 1:1 ratio. pRBC stimulated cells were used to assess malaria specific responses, and uRBC stimulated
567 cells were used to phenotype all Tfh cells. PBMCs were stained with antibodies against CD49b and
568 LAG-3 along with Fc block for 45 minutes at 37C, 5% CO_2. Following 2 washes with PBS, cells were
569 then stained with LIVE/DEAD Fixable Blue Dead Cell Stain for 15 minutes at room temperature,

570 washed twice with 2% FCS/PBS, and then surface stained for 15 minutes at room temperature with
571 fluorescent-tagged antibodies from Biolegend (CA, USA), and BD Biosciences (CA, USA)
572 (**Supplementary Table S3**) e. After 2 washes with 2% FCS/PBS Cells were fixed and permeabilized
573 with eBioscienceTM Foxp3 / Transcription Factor Staining Buffer Set (Thermo Fisher Scientific
574 (MA, USA); Cat. #00-5523-00) solution for 20 minutes on ice. After 2 washes with 1X perm buffer,
575 intracellular staining was performed for 30 minutes on ice with fluorescent-tagged antibodies from
576 Biolegend (CA, USA), and BD Biosciences (CA, USA) (**Supplementary Table S3**). Cells were re-
577 suspended in 2% FCS/PBS, and events were collected on the Cytek Aurora 5 laser cytometer (CA,
578 USA).

579 **PMA stimulation and intracellular cytokine staining**

580 Approximately 1 x 10^6 PBMCs were used per patient per condition/ stain. Thawing of cryopreserved
581 PBMCs was done as previously described. For cytokine induction following PMA and Ionomycin
582 stimulation, PBMC samples were rested overnight in 10% FCS/RPMI after thawing. After rest,
583 PBMCs were stimulated with PMA (25 ng/ mL; Sigma) and Ionomycin (1 ug/mL; Sigma) for 6 hours
584 at 37°C, 5% CO2. Brefeldin A (10 ug/mL; BD Biosciences) and monensin (10 ug/mL; BD
585 Biosciences) were added after the first 2 hours of stimulation. To account for downregulation of
586 chemokine receptors after exposure to BFA and monensin, antibodies against CCR7, CXCR3,
587 CXCR5 and CCR6 were added alongside Fc block during stimulation with PMA/Ionomycin, prior to
588 addition of BFA and monensin. Anti-CD107a was also included during stimulation for intracellular
589 capture. After stimulation, cells were washed with PBS and stained at room temperature for
590 15 minutes with LIVE/DEAD Fixable Blue Dead Cell Stain, washed twice with 2% FCS/PBS, and
591 then surface stained with the antibodies listed in **Supplementary Table S4** for 15 minutes at room
592 temperature. Following 2 washes with 2% FCS/PBS, cells underwent fixation/permeabilization with
593 eBioscience Fixation/Permeabilization solution for 20 minutes on ice and washed in permeabilization
594 buffer. Intracellular staining (ICS) with the antibodies listed in **Supplementary Table S4** was
595 performed for 30 minutes on ice following washes with permeabilization buffer and then fixed with
596 BD stabilizing fixative. Samples were acquired on Cytek Aurora 5.

597 **Flow cytometry data analysis**

598 Flow cytometry data was analysed using FlowJo v10 and then analysed on R (version 4.4.2). For
599 unsupervised data analysis, spectre (version 1.2.0) was used [56].

600 **Single Cell RNA sequencing and analysis**

601 *Cell isolation*

602 Healthy reference data set – PBMCs from four healthy donors were thawed in thawed in RPMI 1640
603 (Gibco) containing 10% FCS and 0.02% Benzonase. Cells were rested for 2 hours in 10% FCS/PBS at
604 37C, 5% CO_2. After rest, untouched CD4+ T cells were enriched from PBMCs using the CD4+ T cell
605 isolation kit (Miltenyi). Enriched CD4+ T cells were then incubated with Fc block for 15 minutes and
606 then surface stained with antibodies listed in **Supplementary Table S8** for 15 minutes at room
607 temperature. Cells were washed with 0.5% BSA/PBS and stained for viability with Sytox Blue
608 (Invitrogen (CA, USA), Cat. # S34857) and sorted on BD FACSAria™III Cell Sorter into 0.5%
609 BSA/PBS. Four populations of cells were sorted, PD1- Tfh (nnCD4/CXCR5+/PD1-), pTfh1
610 (nnCD4/CXCR5+/PD1+/CXCR3+ CCR6-), pTfh2 (nnCD4/CXCR5+/PD1+/CXCR3- CCR6-) and
611 pTfh17 (nnCD4/CXCR5+/PD1+/CXCR3- CCR6+). After sorting, cells of a single phenotype were
612 pooled and run on a single 10X Chromium lane.

613 CHMI – PBMCs collected at day 0, 8, 16, 36 from four participants in CHMI study NCT02867059 [53]
614 were thawed in RPMI 1640 (Gibco) containing 10% FCS and 0.02% Benzonase. Cells were
615 washed with 0.5% BSA/PBS and then incubated with Fc block and antibodies against pan-gD and
616 CXCR5 for 15 minutes at room temperature. Following that, the other antibodies listed in Stain 2 in
617 **Supplementary Table S9** were added and cells were incubated for another 15 minutes at room
618 temperature. Cells were washed and stained for viability with Sytox Blue (Invitrogen (CA, USA), Cat.
619 # S34857) and sorted on BD FACSAria™III Cell Sorter into 0.5% BSA/PBS. Live Tfh cells were
620 sorted as nnCD4, CXCR5+PD1+ cells. After sorting, cells from a single time point were pooled and
621 run on a single 10X Chromium lane.

622 *10 X Genomics Chromium GEX Library preparation and sequencing*

623 Sorted cells were loaded into each lane of Chromium Next GEM Single Cell 5' Reagent Kit v2 and
624 Gel Bead-in- Emulsion (GEMs) generated in the 10X Chromium Controller (Chromium Next GEM
625 Single Cell 5' Kit v2, PN-1000263, Chromium Single cell V(D)J Amplification Kits: Human TCR,
626 PN-1000252, Chromium Next GEM Chip K Single Cell Kit, PN-1000286, , Dual Index Kit TT Set
627 A, PN-1000215). 5' Gene Expression
628 Libraries and VDJ libraries (TCR) were generated according to the manufacturer's instructions.
629 Generated libraries were sequenced in a NextSeq 550 System using High Output Kit (150 Cycles)
630 version 1 according to the manufacturer's protocol using paired-end sequencing (150-bp Read 1 and
631 150 bp Read 2) with the following parameters Read 1: 26 cycles, i7 index: 10 cycles, i5 index: 10
632 cycles and Read 2: 90 cycles.
633 *Demultiplexing and analysis*

634 ScRNAseq data was demultiplexed, aligned and quantified using Cell Ranger version 3.1.0 software
635 (10x Genomics) against the human reference genome (GRCh38-3.0.0) with default parameters. Cell
636 genotype was obtained using cellsnp-lite [57] with the list of informative SNPs obtained from
637 1000_Genome_Project [58]. Then vireo was used to predict the original donor utilising the cell's
638 haplotype ratios, only predicted singlets were used for the analysis [59]. Cell ranger count matrices for
639 each sample were loaded, merged and analysed using Seurat package v4.3.0 and v5.1.0 [60] and
640 visualised with scCustomize v3.0.1 [61]. The healthy reference and CHMI datasets were processed as
641 two separate datasets. Cells were filtered to remove those expressing fewer than 200 genes and more
642 than 4000 genes, and those with more than 10% mitochondrial content. Only genes expressed in three
643 or more cells were considered. TRA/TRB gene expression were removed from the GEX dataset prior
644 to further downstream processing.
645 For Healthy Reference map – Dataset was split by donor and then each individual donor dataset was
646 normalised with SCTransform where highly variable genes were also selected. Before integration, the
647 most variable genes shared among the donor datasets were identified using FindintegrationAnchors
648 and were used to integrate the datasets using the IntegrateData function. Following that, PCA

649 dimensionality reduction was performed using RunPCA and the top 20 PCs were used to compute
650 UMAP visualisation using RunUMAP.
651 For CHMI data - Dataset was split per donor and day, then each individual donor_day dataset was
652 normalised with SCTransform where highly variable genes were also selected.[62] Before integration,
653 the most variable genes shared among the datasets were identified using FindIntegrationAnchors and
654 used to integrate the datasets using the IntegrateData function. Following that, PCA dimensionality
655 reduction was performed using RunPCA and the top 20 PCs were used to compute UMAP
656 visualisation using RunUMAP.
657 *Cell cluster annotation*
658 Healthy reference map – We applied unsupervised clustering using the Louvain algorithm as our
659 modularity optimisation technique and set the granularity of clusters at a resolution of 0.3. A cluster
660 with high mitochondrial content and low read counts was removed as it implies a cluster of cells of
661 low quality. RNA-level counts were log-normalised using NormalizeData (scale factor = 10,000 by
662 default) and were used to run FindMarkers for identifying cluster marker genes as part of cluster
663 annotation. This identified the Tfh1 cluster, along with Tfh2, Tfh17 stress, ribosomal, Type I IFN,
664 cluster 2 and cluster 3 clusters. We then visualised the expression of Treg-related genes (*FOXP3* and
665 *IL2RA)* on the map to identify a cluster of cells belonging to Tfreg within Tfh2 cluster, and another
666 subset of Tfh1/17 cluster which expressed *RORC* along with *CXCR3*, that were positioned separately
667 from the main Tfh1 cluster. Further sub-clustering was also attempted on each of the main Tfh1/2/17
668 clusters separately to identify any higher-level annotations/groupings that could exist within each
669 subset, however only 2 sub-clusters within the Tfh1 subset were suggested to be of functional
670 difference. Automated cell labelling tool, scType [35], was used to transfer labels from the healthy
671 reference Tfh map onto a published human tonsil Tfh dataset [26] containing non-GC and GC Tfh
672 subsets. Detailed steps of how the label transfer was performed is as per described below in CHMI
673 data section. Cluster markers of each cluster were further analysed for pathway enrichment using the
674 Ingenuity Pathway Analysis (IPA) suite (v01-22-01, QIAGEN, DUS, Germany).

675 CHMI data – Unsupervised clustering was calculated using Louvain algorithm with resolution set at
676 2.2 to achieve overclustering. Low-quality clusters with high mitochondrial content and low read
677 counts were removed. Label transfer using cell type annotations from the Healthy Reference Map
678 onto the CMHI dataset was performed using scType [35]. The top 20 up- and down-regulated cluster
679 marker genes from each reference cell type were used to calculate a specificity score to predict the
680 cell type for each cluster in the CHMI dataset. Based on the final top-specificity score, similar clusters
681 are then stitched together for the final annotation. As an additional quality check step, a fold-change
682 between the score of the top-predicted cell type versus every other possible cell type was calculated
683 per cluster, and any cluster where the difference between the top-predicted cell type and the next
684 possible cell type was less than 1.1 was flagged as "low confidence". For clusters 14, 19 and 22 where
685 the top-predicted cell type was flagged as "low-confidence", a manual comparison of key cell type
686 marker genes was done to confirm the final cell annotation used (final annotation: cluster 14 as
687 Tfh1_CCR7, cluster 19 as cluster 2, cluster 22 as Tfh1_Cyto). After the final prediction, we visualised
688 Treg markers (*"Il2ra", "Foxp3"*) and manually selected for an area on the UMAP with high
689 expression of these markers as "Tfr" cluster. For the reference database, we omitted Tfh1/17 and Tfr
690 as input as these 2 clusters had signatures commonly shared with the other clusters: Tfh1/17 with
691 Tfh1 and Tfh17, and Tfreg with Tfh2. RNA-level counts were log-normalised using NormalizeData
692 (scale factor = 10,000 by default) and were used to run FindMarkers for identifying additional cluster
693 marker genes for each annotated cluster.

694 *Pseudobulked Differential Gene Expression Analysis and Pathway Analysis*

695 The normalised count matrix and the metadata were extracted from the Seurat object. Counts were
696 aggregated per sample (i.e. donor and day) for each cluster. Since we conducted a paired-wise
697 comparison (e.g. day 0 vs day 16) only clusters present in both samples were included in the analysis.
698 Significant genes were determined using the quasi-likelihood (QL) F-test with an FDR< 0.05 using
699 edgeR [63]. Aggregated counts were used for visualising changes in specific DEGs using
700 ComplexHeatmap.

701 *TCRA/B clonal analysis*

Annotated TCR sequences were integrated with the single-cell transcriptomics data using the combineTCR and combineExpression functions from scRepertoire (version 2.0.0). The CDR3 amino acid sequences were used to call and quantify clones. Only cells with single and complete paired TCRA and TCRB chain were included. The R package circlize (v0.4.16) and clonalOverlap function of scRepertoire were used to generate the circos and heatmap plots of clonal overlap, respectively. For Simpson's diversity index calculations, data were down-sampled to 1,000 cells to adjust for cell count variations between samples.

Statistical analysis

Non-parametric testing was performed for all analysis. Continuous data for all cellular responses were compared between groups using Mann-Whitney U test, or in paired samples with Wilxcox paired sign-rank test, or correlated with antibody score as a continuous variable with Spearman's correlations. Statistical comparisons were adjusted for multiple comparisons where indicated. All analyses were performed in R (version 4.4.2). Graphical outputs were made in ggplot2 (version 3.5.1) and ggpubr (version 0.6.0). No sample size calculation was performed, instead all available participant data was included. Due to sample size restrictions, no subgroup analysis was performed. Data generation was performed with blinding to participant demographic data.

Data and code availability

All data generated or analysed during this study are included in this article and supplementary information files or deposited online as follows. The raw sequencing data and processed Cell Ranger outputs used in this study have been deposited in the NCBI data base under accession code GSE272939 https://www.ncbi.nlm.nih.gov/geo/query/acc.cgi?acc=GSE272939 and GSE253661 https://www.ncbi.nlm.nih.gov/geo/query/acc.cgi?acc=GSE253661.

The processed single cell RNA sequencing data are available in the Zenodo, https://doi.org/10.5281/zenodo.14847353.

Code used to analyse scRNAseq data is available at https://github.com/MichelleBoyle/CCR7-expression-defines-distinct-pTfh1-subsets-involved-in-malaria-immunity.git

728 Flow cytometry files will be made freely available on publication in an online repository.

729

730 **Author contributions**

731 MSFS, ND, RM, DA, JRL and JAC generated data, supervised by JGB, CE, AH and MJB

732 MSFS, DAO, ZP analysed data

733 JM provided clinical samples used in this study

734 AH and MJB conceptualised study

735 MSFS and MJB led manuscript writing.

736 All authors contributed to and approved manuscript

737

738 **Declarations of interest**

739 All authors declare no conflicts of interest

740

741 **Acknowledgements**

742 Burnet Institute, University of Melbourne and QIMR-Berghofer acknowledge the traditional
743 custodians of the lands where they are located, the Boonwurrung and Wurundjeri Woi-wurrong
744 people of the Kulin Nation, and the Turrbal and Jagera people.

745 RBC and human serum were provided by the Australian Red Cross Blood Bank (Melbourne and
746 Brisbane). We thank the participants involved in the CHMI studies and all study clinicians and
747 support staff at QPharm.

748 This work was supported by the National Health and Medical Research Council of Australia (program
749 grant 1132975 to J.S.M and C.R.E.); Senior Research Fellowships C.R.E. (1154265), Career
750 Development Award 1141278, Project Grant 1125656, and Ideas Grant 1181932 to MJB); the CSL

751 Centenary Fellowship and the Snow Medical Foundation Fellowship 2022/SF167 to M.J.B; the Jim
752 and Margaret Beever Fellowship to J.A.C. The Burnet Institute is supported by the NHMRC for
753 Independent Research Institutes Infrastructure Support Scheme and the Victorian State Government
754 Operational Infrastructure Support. Medicines for Malaria Venture funded the parent CHMI studies.

755

756

757

758 **References**

759

760 1. Geneva: World Health Organisation (2023). World malaria report 2023
761 Geneva: World Health Organisation, ed.

762 2. Datoo, M.S., Dicko, A., Tinto, H., Ouédraogo, J.-B., Hamaluba, M., Olotu, A., Beaumont,
763 E., Lopez, F.R., Natama, H.M., Weston, S., et al. (2024). Safety and efficacy of malaria
764 vaccine candidate R21/Matrix-M in African children: a multicentre, double-blind,
765 randomised, phase 3 trial. Lancet *403*, 533–544. https://doi.org/10.1016/s0140-
766 6736(23)02511-4.

767 3. The RTS,S Clinical Trials Partnership (2014). Efficacy and Safety of the RTS,S/AS01
768 Malaria Vaccine during 18 Months after Vaccination: A Phase 3 Randomized, Controlled
769 Trial in Children and Young Infants at 11 African Sites. PLoS Med. *11*, e1001685.
770 https://doi.org/10.1371/journal.pmed.1001685.

771 4. Yu, D., Walker, L.S.K., Liu, Z., Linterman, M.A., and Li, Z. (2022). Targeting TFH cells
772 in human diseases and vaccination: rationale and practice. Nat. Immunol. *23*, 1157–1168.
773 https://doi.org/10.1038/s41590-022-01253-8.

774 5. Olatunde, A.C., Hale, J.S., and Lamb, T.J. (2021). Cytokine-skewed Tfh cells: functional
775 consequences for B cell help. Trends Immunol. *42*, 536–550.
776 https://doi.org/10.1016/j.it.2021.04.006.

777 6. Vella, L.A., Buggert, M., Manne, S., Herati, R.S., Sayin, I., Kuri-Cervantes, L., Brody,
778 I.B., O'Boyle, K.C., Kaprielian, H., Giles, J.R., et al. (2019). T follicular helper cells in
779 human efferent lymph retain lymphoid characteristics. The Journal of clinical investigation
780 *129*, 3185–3200. https://doi.org/10.1172/jci125628.

781 7. Dalit, L., Tan, C.W., Sheikh, A.A., Munnings, R., Alvarado, C., Hussain, T., Zaini, A.,
782 Cooper, L., Kirn, A., Hailes, L., et al. (2024). Divergent cytokine and transcriptional
783 signatures control functional T follicular helper cell heterogeneity. bioRxiv,
784 2024.06.12.598622. https://doi.org/10.1101/2024.06.12.598622.

785 8. Locci, M., Havenar-Daughton, C., Landais, E., Wu, J., Kroenke, M.A., Arlehamn, C.L.,
786 Su, L.F., Cubas, R., Davis, M.M., Sette, A., et al. (2013). Human Circulating PD-1+CXCR3-
787 CXCR5+ Memory Tfh Cells Are Highly Functional and Correlate with Broadly Neutralizing
788 HIV Antibody Responses. Immunity *39*, 758–769.
789 https://doi.org/10.1016/j.immuni.2013.08.031.

790 9. Bentebibel, S.-E., Lopez, S., Obermoser, G., Schmitt, N., Mueller, C., Harrod, C., Flano,
791 E., Mejias, A., Albrecht, R.A., Blankenship, D., et al. (2013). Induction of
792 ICOS+CXCR3+CXCR5+ TH Cells Correlates with Antibody Responses to Influenza
793 Vaccination. Sci. Transl. Med. *5*, 176ra32. https://doi.org/10.1126/scitranslmed.3005191.

794 10. Bentebibel, S.-E., Khurana, S., Schmitt, N., Kurup, P., Mueller, C., Obermoser, G.,
795 Palucka, A.K., Albrecht, R.A., Garcia-Sastre, A., Golding, H., et al. (2016). ICOS+PD-

796 1+CXCR3+ T follicular helper cells contribute to the generation of high-avidity antibodies
797 following influenza vaccination. Sci. Rep. *6*, 26494. https://doi.org/10.1038/srep26494.

798 11. Soon, M.S.F., Nalubega, M., and Boyle, M.J. (2021). T-follicular helper cells in malaria
799 infection and roles in antibody induction. Oxf Open Immunol *2*, iqab008-.
800 https://doi.org/10.1093/oxfimm/iqab008.

801 12. Chan, J.-A., Loughland, J.R., Rivera, F. de L., SheelaNair, A., Andrew, D.W., Dooley,
802 N.L., Wines, B.D., Amante, F.H., Webb, L., Hogarth, P.M., et al. (2020). Th2-like T
803 Follicular Helper Cells Promote Functional Antibody Production during Plasmodium
804 falciparum Infection. Cell Reports Medicine *1*, 100157.
805 https://doi.org/10.1016/j.xcrm.2020.100157.

806 13. Bowyer, G., Grobbelaar, A., Rampling, T., Venkatraman, N., Morelle, D., Ballou, R.W.,
807 Hill, A.V.S., and Ewer, K.J. (2018). CXCR3+ T Follicular Helper Cells Induced by Co-
808 Administration of RTS,S/AS01B and Viral-Vectored Vaccines Are Associated With Reduced
809 Immunogenicity and Efficacy Against Malaria. Front Immunol *9*, 1660.
810 https://doi.org/10.3389/fimmu.2018.01660.

811 14. Nielsen, C.M., Ogbe, A., Pedroza-Pacheco, I., Doeleman, S.E., Chen, Y., Silk, S.E.,
812 Barrett, J.R., Elias, S.C., Miura, K., Diouf, A., et al. (2021). Protein/AS01B vaccination
813 elicits stronger, more Th2-skewed antigen-specific human T follicular helper cell responses
814 than heterologous viral vectors. Cell Reports Medicine, 100207.
815 https://doi.org/10.1016/j.xcrm.2021.100207.

816 15. Minassian, A.M., Silk, S.E., Barrett, J.R., Nielsen, C.M., Miura, K., Diouf, A., Loos, C.,
817 Fallon, J.K., Michell, A.R., White, M.T., et al. (2021). Reduced blood-stage malaria growth
818 and immune correlates in humans following RH5 vaccination. Med *2*, 701-719.e19.
819 https://doi.org/10.1016/j.medj.2021.03.014.

820 16. Oyong, Damian.A., Loughland, Jessica.R., Soon, Megan.S.F., Chan, J.-A., Andrew, D.,
821 Wines, B.D., Hogarth, P.M., Olver, S.D., Collinge, A.D., Varelias, A., et al. (2022). Adults
822 with Plasmodium falciparum malaria have higher magnitude and quality of circulating T-
823 follicular helper cells compared to children. Ebiomedicine *75*, 103784.
824 https://doi.org/10.1016/j.ebiom.2021.103784.

825 17. Obeng-Adjei, N., Portugal, S., Tran, T.M., Yazew, T.B., Skinner, J., Li, S., Jain, A.,
826 Felgner, P.L., Doumbo, O.K., Kayentao, K., et al. (2015). Circulating Th1-Cell-type Tfh
827 Cells that Exhibit Impaired B Cell Help Are Preferentially Activated during Acute Malaria in
828 Children. CellReports *13*, 425–439. https://doi.org/10.1016/j.celrep.2015.09.004.

829 18. Vijay, R., Guthmiller, J.J., Sturtz, A.J., Surette, F.A., Rogers, K.J., Sompallae, R.R., Li,
830 F., Pope, R.L., Chan, J.-A., Rivera, F. de L., et al. (2020). Infection-induced plasmablasts are
831 a nutrient sink that impairs humoral immunity to malaria. Nat Immunol *21*, 790–801.
832 https://doi.org/10.1038/s41590-020-0678-5.

833 19. Chan, J.-A., Loughland, J.R., Parte, L. de la, Okano, S., Ssewanyana, I., Nalubega, M.,
834 Nankya, F., Musinguzi, K., Rek, J., Arinaitwe, E., et al. (2022). Age-dependent changes in
835 circulating Tfh cells influence development of functional malaria antibodies in children. Nat
836 Commun *13*, 4159. https://doi.org/10.1038/s41467-022-31880-6.

837 20. Obeng-Adjei, N., Portugal, S., Holla, P., Li, S., Sohn, H., Ambegaonkar, A., Skinner, J.,
838 Bowyer, G., Doumbo, O.K., Traore, B., et al. (2017). Malaria-induced interferon-γ drives the
839 expansion of Tbethi atypical memory B cells. PLoS pathogens *13*, e1006576.
840 https://doi.org/10.1371/journal.ppat.1006576.

841 21. Opi, D.H., Kurtovic, L., Chan, J.-A., Horton, J.L., Feng, G., and Beeson, J.G. (2021).
842 Multi-functional antibody profiling for malaria vaccine development and evaluation. Expert
843 Rev Vaccines *20*, 1257–1272. https://doi.org/10.1080/14760584.2021.1981864.

844 22. Xu, W., Zhao, X., Wang, X., Feng, H., Gou, M., Jin, W., Wang, X., Liu, X., and Dong, C.
845 (2019). The Transcription Factor Tox2 Drives T Follicular Helper Cell Development via
846 Regulating Chromatin Accessibility. Immunity *51*, 826-839.e5.
847 https://doi.org/10.1016/j.immuni.2019.10.006.

848 23. Horiuchi, S., Wu, H., Liu, W.-C., Schmitt, N., Provot, J., Liu, Y., Bentebibel, S.-E.,
849 Albrecht, R.A., Schotsaert, M., Forst, C.V., et al. (2021). Tox2 is required for the
850 maintenance of GC TFH cells and the generation of memory TFH cells. Sci Adv *7*, eabj1249.
851 https://doi.org/10.1126/sciadv.abj1249.

852 24. Kroenke, M.A., Eto, D., Locci, M., Cho, M., Davidson, T., Haddad, E.K., and Crotty, S.
853 (2012). Bcl6 and Maf Cooperate To Instruct Human Follicular Helper CD4 T Cell
854 Differentiation. J. Immunol. *188*, 3734–3744. https://doi.org/10.4049/jimmunol.1103246.

855 25. Andris, F., Denanglaire, S., Anciaux, M., Hercor, M., Hussein, H., and Leo, O. (2017).
856 The Transcription Factor c-Maf Promotes the Differentiation of Follicular Helper T Cells.
857 Front. Immunol. *8*, 480. https://doi.org/10.3389/fimmu.2017.00480.

858 26. Massoni-Badosa, R., Aguilar-Fernández, S., Nieto, J.C., Soler-Vila, P., Elosua-Bayes, M.,
859 Marchese, D., Kulis, M., Vilas-Zornoza, A., Bühler, M.M., Rashmi, S., et al. (2024). An atlas
860 of cells in the human tonsil. Immunity. https://doi.org/10.1016/j.immuni.2024.01.006.

861 27. Cook, M.E., Shchukina, I., Lin, C.-C., Bradstreet, T.R., Schwarzkopf, E.A., Jarjour, N.N.,
862 Webber, A.M., Zaitsev, K., Artyomov, M.N., and Edelson, B.T. (2023). BHLHE40 Mediates
863 Cross-Talk between Pathogenic TH17 Cells and Myeloid Cells during Experimental
864 Autoimmune Encephalomyelitis. ImmunoHorizons *7*, 737–746.
865 https://doi.org/10.4049/immunohorizons.2300042.

866 28. Lin, C.-C., Bradstreet, T.R., Schwarzkopf, E.A., Jarjour, N.N., Chou, C., Archambault,
867 A.S., Sim, J., Zinselmeyer, B.H., Carrero, J.A., Wu, G.F., et al. (2016). IL-1–induced
868 Bhlhe40 identifies pathogenic T helper cells in a model of autoimmune neuroinflammation. J.
869 Exp. Med. *213*, 251–271. https://doi.org/10.1084/jem.20150568.

870 29. Hatton, R.D. (2011). TGF-β in Th17 Cell Development: The Truth Is Out There.
871 Immunity *34*, 288–290. https://doi.org/10.1016/j.immuni.2011.03.009.

872 30. Xie, M.M., Fang, S., Chen, Q., Liu, H., Wan, J., and Dent, A.L. (2019). Follicular
873 regulatory T cells inhibit the development of granzyme B-expressing follicular helper T cells.
874 JCI insight *4*. https://doi.org/10.1172/jci.insight.128076.

875 31. Liang, C., Spoerl, S., Xiao, Y., Habenicht, K.M., Haeusl, S.S., Sandner, I., Winkler, J.,
876 Strieder, N., Eder, R., Stanewsky, H., et al. (2024). Oligoclonal CD4+CXCR5+ T cells with a
877 cytotoxic phenotype appear in tonsils and blood. Commun. Biol. *7*, 879.
878 https://doi.org/10.1038/s42003-024-06563-1.

879 32. Kumar, S., Basto, A.P., Ribeiro, F., Almeida, S.C.P., Campos, P., Peres, C., Pulvirenti,
880 N., Al-Khalidi, S., Kilbey, A., Tosello, J., et al. (2024). Specialized Tfh cell subsets driving
881 type-1 and type-2 humoral responses in lymphoid tissue. Cell Discov. *10*, 64.
882 https://doi.org/10.1038/s41421-024-00681-0.

883 33. He, J., Tsai, L.M., Leong, Y.A., Hu, X., Ma, C.S., Chevalier, N., Sun, X., Vandenberg,
884 K., Rockman, S., Ding, Y., et al. (2013). Circulating Precursor CCR7loPD-1hi CXCR5+
885 CD4+ T Cells Indicate Tfh Cell Activity and Promote Antibody Responses upon Antigen
886 Reexposure. Immunity *39*, 770–781. https://doi.org/10.1016/j.immuni.2013.09.007.

887 34. Crotty, S. (2014). T Follicular Helper Cell Differentiation, Function, and Roles in
888 Disease. Immunity *41*, 529–542. https://doi.org/10.1016/j.immuni.2014.10.004.

889 35. Ianevski, A., Giri, A.K., and Aittokallio, T. (2022). Fully-automated and ultra-fast cell-
890 type identification using specific marker combinations from single-cell transcriptomic data.
891 Nat. Commun. *13*, 1246. https://doi.org/10.1038/s41467-022-28803-w.

892 36. Smith, N.P., Ruiter, B., Virkud, Y.V., Tu, A.A., Monian, B., Moon, J.J., Love, J.C., and
893 Shreffler, W.G. (2021). Identification of antigen-specific TCR sequences based on biological
894 and statistical enrichment in unselected subjects. JCI Insight *6*, e140028.
895 https://doi.org/10.1172/jci.insight.140028.

896 37. Venturi, V., Kedzierska, K., Price, D.A., Doherty, P.C., Douek, D.C., Turner, S.J., and
897 Davenport, M.P. (2006). Sharing of T cell receptors in antigen-specific responses is driven by
898 convergent recombination. Proc. Natl. Acad. Sci. *103*, 18691–18696.
899 https://doi.org/10.1073/pnas.0608907103.

900 38. Zheng, M.Z.M., Burmas, L., Tan, H.-X., Trieu, M.-C., Lee, H.J., Rawlinson, D., Haque,
901 A., Kent, S.J., Wheatley, A.K., and Juno, J.A. (2024). Deconvoluting TCR-dependent & -
902 independent activation is vital for reliable Ag-specific CD4+ T cell characterization by AIM
903 assay. bioRxiv, 2024.12.10.627643. https://doi.org/10.1101/2024.12.10.627643.

904 39. Wahl, I., Obraztsova, A.S., Puchan, J., Hundsdorfer, R., Chakravarty, S., Sim, B.K.L.,
905 Hoffman, S.L., Kremsner, P.G., Mordmüller, B., and Wardemann, H. (2022). Clonal
906 evolution and TCR specificity of the human TFH cell response to Plasmodium falciparum
907 CSP. Sci Immunol *7*, eabm9644. https://doi.org/10.1126/sciimmunol.abm9644.

908 40. Morita, R., Schmitt, N., Bentebibel, S.-E., Ranganathan, R., Bourdery, L., Zurawski, G.,
909 Foucat, E., Dullaers, M., Oh, S., Sabzghabaei, N., et al. (2011). Human blood
910 CXCR5(+)CD4(+) T cells are counterparts of T follicular cells and contain specific subsets
911 that differentially support antibody secretion. Immunity *34*, 108–121.
912 https://doi.org/10.1016/j.immuni.2010.12.012.

913 41. Juno, J.A., Tan, H.-X., Lee, W.S., Reynaldi, A., Kelly, H.G., Wragg, K., Esterbauer, R.,
914 Kent, H.E., Batten, C.J., Mordant, F.L., et al. (2020). Humoral and circulating follicular

915 helper T cell responses in recovered patients with COVID-19. Nature medicine, 1–22.
916 https://doi.org/10.1038/s41591-020-0995-0.

917 42. Wong, M.T., Chen, J., Narayanan, S., Lin, W., Anicete, R., Kiaang, H.T.K., Lafaille,
918 M.A.C.D., Poidinger, M., and Newell, E.W. (2015). Mapping the Diversity of Follicular
919 Helper T Cells in Human Blood and Tonsils Using High-Dimensional Mass Cytometry
920 Analysis. CellReports *11*, 1822–1833. https://doi.org/10.1016/j.celrep.2015.05.022.

921 43. Dan, J.M., Havenar-Daughton, C., Kendric, K., Al-Kolla, R., Kaushik, K., Rosales, S.L.,
922 Anderson, E.L., LaRock, C.N., Vijayanand, P., Seumois, G., et al. (2019). Recurrent group A
923 Streptococcus tonsillitis is an immunosusceptibility disease involving antibody deficiency
924 and aberrant TFH cells. Science translational medicine *11*.
925 https://doi.org/10.1126/scitranslmed.aau3776.

926 44. Lederer, K., Bettini, E., Parvathaneni, K., Painter, M.M., Agarwal, D., Lundgreen, K.A.,
927 Weirick, M., Muralidharan, K., Castano, D., Goel, R.R., et al. (2022). Germinal center
928 responses to SARS-CoV-2 mRNA vaccines in healthy and immunocompromised individuals.
929 Cell. https://doi.org/10.1016/j.cell.2022.01.027.

930 45. Nelson, C.S., and Sage, P.T. (2024). TFH cell responses endure in human lymph nodes
931 after vaccination. Nat. Immunol., 1–3. https://doi.org/10.1038/s41590-024-01935-5.

932 46. Mudd, P.A., Minervina, A.A., Pogorelyy, M.V., Turner, J.S., Kim, W., Kalaidina, E.,
933 Petersen, J., Schmitz, A.J., Lei, T., Haile, A., et al. (2022). SARS-CoV-2 mRNA vaccination
934 elicits a robust and persistent T follicular helper cell response in humans. Cell *185*, 603-
935 613.e15. https://doi.org/10.1016/j.cell.2021.12.026.

936 47. Borcherding, N., Kim, W., Quinn, M., Han, F., Zhou, J.Q., Sturtz, A.J., Schmitz, A.J.,
937 Lei, T., Schattgen, S.A., Klebert, M.K., et al. (2024). CD4+ T cells exhibit distinct
938 transcriptional phenotypes in the lymph nodes and blood following mRNA vaccination in
939 humans. Nat. Immunol., 1–11. https://doi.org/10.1038/s41590-024-01888-9.

940 48. Schattgen, S.A., Turner, J.S., Ghonim, M.A., Crawford, J.C., Schmitz, A.J., Kim, H.,
941 Zhou, J.Q., Awad, W., Mettelman, R.C., Kim, W., et al. (2024). Influenza vaccination
942 stimulates maturation of the human T follicular helper cell response. Nat. Immunol., 1–12.
943 https://doi.org/10.1038/s41590-024-01926-6.

944 49. Kho, S., Qotrunnada, L., Leonardo, L., Andries, B., Wardani, P.A.I., Fricot, A., Henry,
945 B., Hardy, D., Margyaningsih, N.I., Apriyanti, D., et al. (2021). Hidden Biomass of Intact
946 Malaria Parasites in the Human Spleen. New Engl J Med *384*, 2067–2069.
947 https://doi.org/10.1056/nejmc2023884.

948 50. Kho, S., Qotrunnada, L., Leonardo, L., Andries, B., Wardani, P.A.I., Fricot, A., Henry,
949 B., Hardy, D., Margyaningsih, N.I., Apriyanti, D., et al. (2021). Evaluation of splenic
950 accumulation and colocalization of immature reticulocytes and Plasmodium vivax in
951 asymptomatic malaria: A prospective human splenectomy study. Plos Med *18*, e1003632.
952 https://doi.org/10.1371/journal.pmed.1003632.

953 51. McCarthy, J.S., Sekuloski, S., Griffin, P.M., Elliott, S., Douglas, N., Peatey, C., Rockett,
954 R., O'Rourke, P., Marquart, L., Hermsen, C., et al. (2011). A pilot randomised trial of

955 induced blood-stage Plasmodium falciparum infections in healthy volunteers for testing
956 efficacy of new antimalarial drugs. PLoS ONE *6*, e21914.
957 https://doi.org/10.1371/journal.pone.0021914.

958 52. Rockett, R.J., Tozer, S.J., Peatey, C., Bialasiewicz, S., Whiley, D.M., Nissen, M.D.,
959 Trenholme, K., Carthy, J.S.M., and Sloots, T.P. (2011). A real-time, quantitative PCR
960 method using hydrolysis probes for the monitoring of Plasmodium falciparum load in
961 experimentally infected human volunteers. Malaria Journal *10*, 48.
962 https://doi.org/10.1186/1475-2875-10-48.

963 53. Gaur, A.H., McCarthy, J.S., Panetta, J.C., Dallas, R.H., Woodford, J., Tang, L., Smith,
964 A.M., Stewart, T.B., Branum, K.C., Freeman, B.B., et al. (2020). Safety, tolerability,
965 pharmacokinetics, and antimalarial efficacy of a novel Plasmodium falciparum ATP4
966 inhibitor SJ733: a first-in-human and induced blood-stage malaria phase 1a/b trial. Lancet
967 Infect. Dis. *20*, 964–975. https://doi.org/10.1016/s1473-3099(19)30611-5.

968 54. McCarthy, J.S., Donini, C., Chalon, S., Woodford, J., Marquart, L., Collins, K.A.,
969 Rozenberg, F.D., Fidock, D.A., Cherkaoui-Rbati, M.H., Gobeau, N., et al. (2020). A Phase 1,
970 Placebo-controlled, Randomized, Single Ascending Dose Study and a Volunteer Infection
971 Study to Characterize the Safety, Pharmacokinetics, and Antimalarial Activity of the
972 Plasmodium Phosphatidylinositol 4-Kinase Inhibitor MMV390048. Clin. Infect. Dis. *71*,
973 e657–e664. https://doi.org/10.1093/cid/ciaa368.

974 55. Collins, K.A., Wang, C.Y., Adams, M., Mitchell, H., Rampton, M., Elliott, S., Reuling,
975 I.J., Bousema, T., Sauerwein, R., Chalon, S., et al. (2018). A controlled human malaria
976 infection model enabling evaluation of transmission-blocking interventions. The Journal of
977 clinical investigation *128*, 1551–1562. https://doi.org/10.1172/jci98012.

978 56. Ashhurst, T.M., Marsh-Wakefield, F., Putri, G.H., Spiteri, A.G., Shinko, D., Read, M.N.,
979 Smith, A.L., and King, N.J.C. (2021). Integration, exploration, and analysis of high-
980 dimensional single-cell cytometry data using Spectre. Cytom Part A.
981 https://doi.org/10.1002/cyto.a.24350.

982 57. Huang, X., and Huang, Y. (2021). Cellsnp-lite: an efficient tool for genotyping single
983 cells. Bioinformatics *37*, 4569–4571. https://doi.org/10.1093/bioinformatics/btab358.

984 58. Consortium, T. 1000 G.P., Auton, A., Abecasis, G.R., Altshuler, D.M., Durbin, R.M.,
985 Abecasis, G.R., Bentley, D.R., Chakravarti, A., Clark, A.G., Donnelly, P., et al. (2015). A
986 global reference for human genetic variation. Nature *526*, 68–74.
987 https://doi.org/10.1038/nature15393.

988 59. Huang, Y., McCarthy, D.J., and Stegle, O. (2019). Vireo: Bayesian demultiplexing of
989 pooled single-cell RNA-seq data without genotype reference. Genome Biol. *20*, 273.
990 https://doi.org/10.1186/s13059-019-1865-2.

991 60. Hao, Y., Stuart, T., Kowalski, M.H., Choudhary, S., Hoffman, P., Hartman, A.,
992 Srivastava, A., Molla, G., Madad, S., Fernandez-Granda, C., et al. (2024). Dictionary learning
993 for integrative, multimodal and scalable single-cell analysis. Nat. Biotechnol. *42*, 293–304.
994 https://doi.org/10.1038/s41587-023-01767-y.

995 61. Marsh, S., Salmon, M., Hoffma, P., and kew24 (2024). samuel-marsh/scCustomize
996 Version 3.0.1 (Zenodo).

997 62. Choudhary, S., and Satija, R. (2022). Comparison and evaluation of statistical error
998 models for scRNA-seq. Genome Biol. *23*, 27. https://doi.org/10.1186/s13059-021-02584-9.

999 63. Robinson, M.D., and Smyth, G.K. (2008). Small-sample estimation of negative binomial
1000 dispersion, with applications to SAGE data. Biostatistics *9*, 321–332.
1001 https://doi.org/10.1093/biostatistics/kxm030.

1002

1003

1004